Ocean Systems Engineering, *Vol. 12, No. 1 (2022) 87-142*
https://doi.org/10.12989/ose.2022.12.1.087

A computer based simulation model for the fatigue damage assessment of deep water marine riser

Chirag A. Pallan[a] and Rajiv Sharma[*]

Design and Simulation Laboratory, Department of Ocean Engineering, IIT Madras, Chennai (TN) - 600036, India

(Received January 8, 2022, Revised March 6, 2022, Accepted March 8, 2022)

Abstract. An analysis for the computation of Fatigue Damage Index (FDI) under the effects of the various combination of the ocean loads like random waves, current, platform motion and VIV (Vortex Induced Vibration) for a certain design water depth is a critically important part of the analysis and design of the marine riser platform integrated system. Herein, a 'Computer Simulation Model (CSM)' is developed to combine the advantages of the frequency domain and time domain. A case study considering a steel catenary riser operating in 1000 m water depth has been conducted with semi-submersible. The riser is subjected to extreme environmental conditions and static and dynamic response analyses are performed and the Response Amplitude Operators (RAOs) of the offshore platform are computed with the frequency domain solution. Later the frequency domain results are integrated with time domain analysis system for the dynamic analysis in time domain. After that an extensive post processing is done to compute the FDI of the marine riser. In the present paper importance is given to the nature of the current profile and the VIV. At the end we have reported the detail results of the FDI comparison with VIV and without VIV under the linear current velocity and the FDI comparison with linear and power law current velocity with and without VIV. We have also reported the design recommendations for the marine riser in the regions where the higher fatigue damage is observed and the proposed CSM is implemented in industrially used standard soft solution systems (i.e., OrcaFlex[*TM] and Ansys AQWA[**TM]), Ms-Excel[***TM], and C++ programming language using its object oriented features.

Keywords: computer simulation model; current velocity; deep water marine riser; fatigue damage; linear law; power law; random waves; vortex induced vibration

1. Introduction

Fatigue is a process in which the material is weakened because of the repeated application of loads. Usually, it is a progressive and localized process, and it causes the structural damage that occurs when the material is subjected to 'cyclic loading'. This cyclic loading is critical in fatigue, and the nominal maximum stress values that can cause fatigue damage are much lower than the material's ultimate tensile stress limit or the yield stress limit. The fatigue occurs when the material is subjected to cyclic loading and unloading, which can cause the reversal of stresses. If the loads are above a certain critical limit (i.e., specific to the material under consideration) then the

∗Corresponding author, Professor, E-mail: rajivatri@iitm.ac.in
[a]Research Scholar, E-mail: chirag.palan@gmail.com

http://www.techno-press.org/?journal=ose&subpage=7 ISSN: 2093-6702 (Print), 2093-677X (Online)

microscopic cracks begin to form at the stress concentrators (i.e., connection points, touch-down points, the surface, persistent slip bands, interfaces of constituents in the case of composites, and grain interfaces in the case of metals, etc.), for more details see Kim and Laird (1978). Slowly, the crack reaches a critical size, and it propagates in any one or all three dimensions these processes of the crack growth and propagation can cause the structure to fracture. The nature of load cycles acting on and the shape of the structure significantly affects the fatigue life, i.e., cyclic loads that can cause the reversal of stresses, periodic and oscillatory loads, square holes, sharp corners etc. lead to the elevated local stresses and at these locations of the high stress the fatigue crack is expected to initiate. Hence, it can be noted here that only the geometric features (i.e. the rounded holes, smooth transitions, and fillets) are in the control of the designer, and other features (i.e., non-cyclic loads, non-random loads, non-periodic and non-oscillatory loads) are dependent upon the ocean environment and they are beyond the control of the designer.

Usually, fatigue is a process that has a degree of randomness (stochastic), and it shows significant deviations even in similar samples in the well-controlled environments. It is governed primarily by the tensile stresses with the secondary fatigue cracks more associated with the compressive stresses, for more details, see (Fleck *et al.* 1985). A more extensive range of the applied stress range reduces the fatigue life, and the fatigue life scatter to increase with the longer fatigue lives. Also, the fatigue damage is cumulative, and the materials will not recover when they are unloaded. From the material science perspective, the fatigue life is controlled by different parameters, i.e., temperature, surface finish, metallurgical microstructure, oxidizing or inert chemicals, residual stresses, and scuffing contact (fretting), etc., for more details, see Varvani-Farahani (2005).

Offshore structures are made of steel, and it exhibits a theoretical fatigue limit below which continued loading does not lead to fatigue failure. However, the high cycle fatigue strength (i.e., for 10^4 to 10^8 loading cycles with frequencies ranging from 20 to 250 Hz) are typically analyzed with the stress based parametric approach and the low cycle fatigue (i.e., for less than 10^4 loading cycles with frequencies ranging from 0.01 to 5 Hz) usually are analyzed with the strain based parametric approach. As the number of loading cycles is significantly large for the offshore structures, a stress-based parametric approach is used for fatigue damage assessment. Because of the reasons mentioned above the, offshore structures are susceptible to fatigue damage. In fact, one of the worst accidents in the history of offshore structures happened because of the fatigue failure, i.e., the capsize of Alexander L. Kielland, Norwegian semi-submersible drilling rig, March 1980, killing 123 people, for more details, see Talka (1981).

A detailed investigation later in March 1981 concluded that the rig collapsed owing to a fatigue crack in one of its six bracings (bracing D-6), and this bracing connected the collapsed D-leg to the rest of the rig. This crack was traced to a small 6 mm fillet weld that joined a non-load-bearing flange plate to the D-6 bracing, as shown in Fig. 1.

This paper focuses on the ‘Computer Simulation Model (CSM)’ for the fatigue damage assessment of deep water marine risers. The remaining of the paper is organized: Section 2 presents a brief and relevant review of previous research works; Section 3 presents some essential mathematical preliminaries about the theory of panel method (frequency domain), finite element analysis of fluid-structure interaction problem (time-domain) and modeling of various loads acting on riser; Section 4 presents the details of a computer-based computational model for modeling semisubmersible and riser in the frequency domain and time domain respectively; Section 5 presents the verification and validation of the proposed computational model with some of the

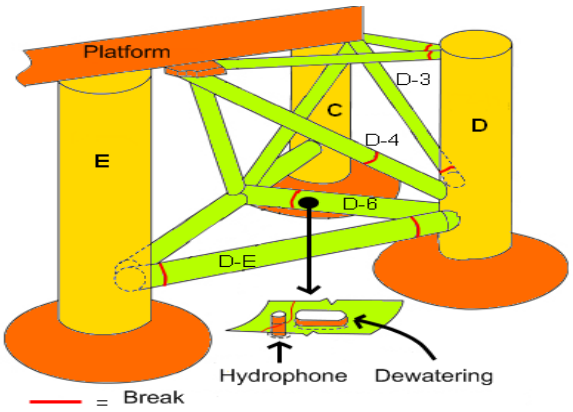

Fig. 1 An illustrated image of the legs of Alexander L. Kielland, Norwegian semi-submersible drilling rig, adapted from Talka (1981)

early published results; Section 6 presents an implementation of numerical example with suitable geometry of semisubmersible and riser; Section 7 presents results and discussion of numerical example; and finally Section 8 concludes the paper and lists the future scope of research. Some of the details have not been reported here to keep the paper of reasonable length. This paper's comprehensive details can be found in Pallan (2019).

1.1 Motivation

In the modern era of high-performance computing simulation and due to the increasing knowledge in a computer simulation, with the help of available techniques like CFD and FEM, now it is possible to model the non-linear complicated industrial problems whose close form solutions are not available. However, even though the high-performance computing tools are available for engineering analyses, at times, they demand a higher memory and computation time, e.g., problems related to fatigue damage assessment for the deep water marine risers. For the problem of interest in this paper, the conventional methods of solution of the fluid-structure interaction problems using the CFD are time-consuming and computationally demanding. Hence, the present study explores an important essential idea of combining the panel method, FEM, and other semi-empirical tools like the wake oscillator model for VIV forces.

1.2 Objective and scope

Herein, the objective is to design and develop a 'Computer Simulation Model (CSM)' for the fatigue damage assessment of deep water marine riser, and we cover the following:

- Investigate the effects of sea states, current velocities with different variations, and the VIV loads on fatigue damage of the marine riser integrated with the offshore platform.
- Investigate the effects of sea states, current velocities with different variations, and the VIV loads on fatigue damage of the marine riser integrated with the offshore platform.
- Investigate the possible computational techniques for better computational efficiency in the marine riser floater coupled problem.

- Investigate the effect of platform motion in all six degrees of freedom on dynamic global response of deep water marine risers.
- Compute numbers of loading cycles and accumulation of damage due to these loading cycles. The loads acting on the marine risers during its operations are described in the coming sections.

2. Brief and relevant review of previous research works

The fatigue analysis of deep water marine riser is a problem of high industrial relevance. Because of its importance, it has been studied extensively in the literature albeit with a highly limited focus, e.g., most of the studies have focused on the effects of current and other forces like the wave and VIV have received only limited attention. This is surprising because most of the offshore locations where marine risers are employed or are expected to be employed are governed by the harsh marine environment, including high sea states and current velocities, and the occurrence of VIV. Various researchers have made some efforts to develop an efficient computational model which can analyze the fatigue behavior and can compute corresponding damage of the deep water marine riser. However, they have been limited because they did not focus on the fatigue analysis under the influence of VIV and coupled offshore platform motion. Although at the theoretical level, 'Fluid-Structure Interaction (FSI)' can handle the inclusion of VIV, which has already been applied to some industries (e.g., aircraft industry), the application in ocean engineering is yet to gain the wider exploration and application. An existing approach uses the CFD to compute the fluid loading on the marine riser and then use the structural analysis to compute the stress time histories and, correspondingly the fatigue damage index. However, in this analysis, there is an important limitation: Feedback about the motion of structures is not taken into consideration efficiently because that demands the use of dynamic mesh generation in the coupled and integrated analysis.

Furthermore, the existing CFD software solution systems like the ANSYS-Work bench^{**TM} can perform a two--way coupled analysis by considering structures' motion feedback. They can generate reasonably good results, albeit with very high computational time, and require proper computing systems (i.e., high-end workstations/desktop PCs). Also, they need higher memory and adaptive meshing strategies and techniques. In the end, there is no guarantee of the solution's convergence and sometime it is highly time-consuming to ensure even a linear convergence, e.g., our attempts for one CFD simulation to produce one second of real-time flow over a 1:100 scaled model of marine riser required almost 20 hours on the computing machine with configuration: HP^{+1} Z420 workstation, Processor: Intel^{+2} Xeon^{+2} @ 3.30 GHz, RAM: 24GB. So, it is essential that some other efficient method is investigated. This thesis is an attempt in that direction.

Herein, the aim is to combine the advantages of FDA (i.e., lesser computational time) and the TDA (i.e., higher accuracy for the dynamic and FSI analysis). The FDA is implemented in the Ansys AQWA^{**TM} and then the results of semi-submersible RAOs are extracted and utilized in the TDA. This is done using the transfer functions while converting the RAOs into the motion time histories. These motion time histories are given as the top end boundary conditions for the TDA. A detailed algorithm in this regard is presented in Fig. 2.

Vandiver and Chung (1988) reported a study on the dynamic response characteristics of a tensioned cable in sheared flow experimentally and proposed a response prediction method for the non-resonance VIV. Usually, the hydrodynamic damping involves 'non-lock-in' modes, and in them, the hydrodynamic damping is around 10 to 100 times the structural damping. Their

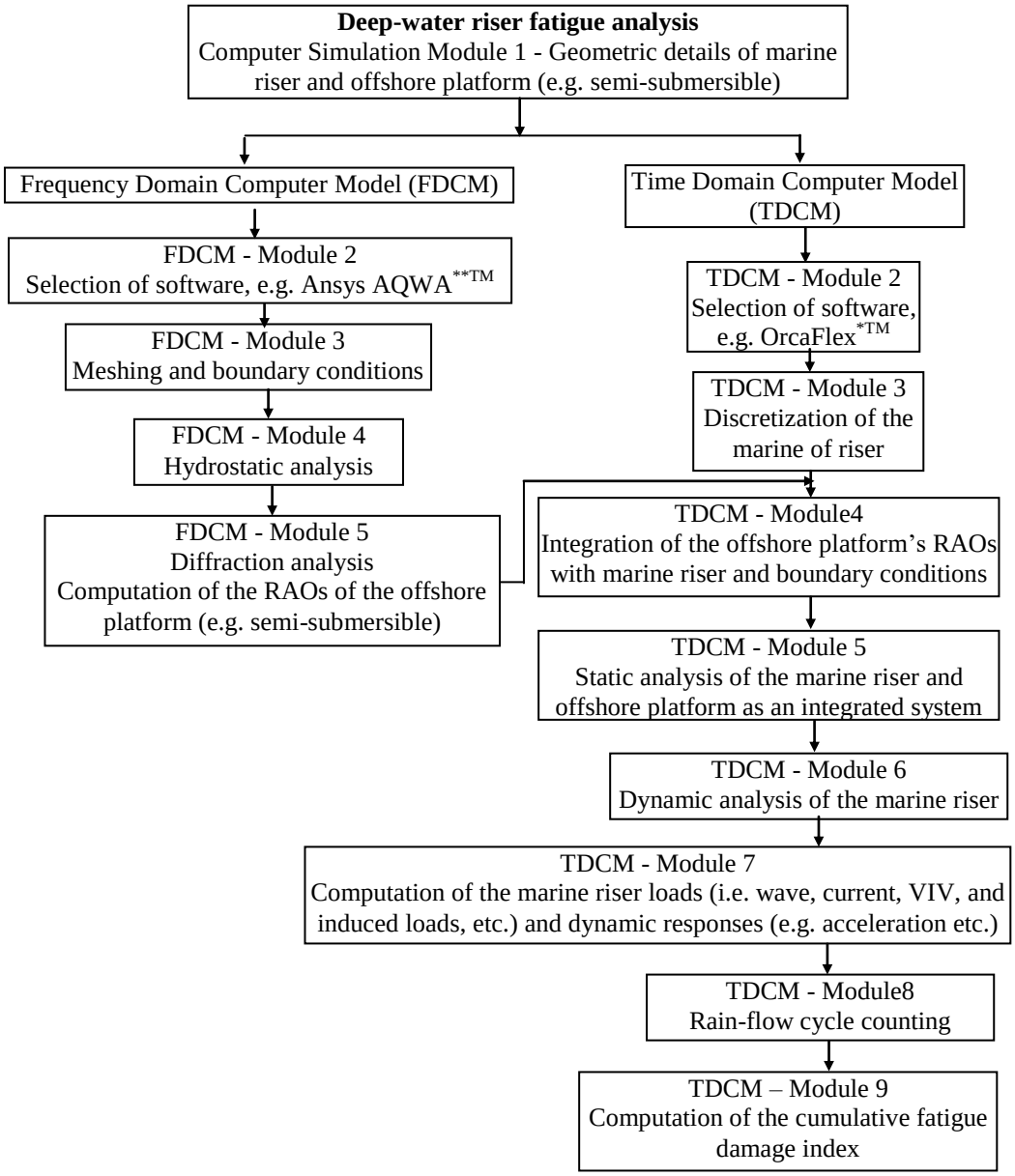

Fig. 2 Modular structure of the proposed CSM for fatigue damage analysis

proposed model can be treated as 2D as well as 3D based upon specific parameters.

Ahmad and Datta (1989) studied the dynamic response of marine riser under both the regular and random waves, and they suggested that the linearized drag under predicts the maximum 'Root Mean Square (RMS)' stress by around 20% to 40%. Also, when the current velocity is added to the water particle velocity, the structural characteristics change drastically, and that implies that the current

has large importance on the marine riser analysis and design.

Bokaian (1990) discussed the effect of boundary conditions on a tensioned beam (i.e., clamped-pinned, pinned-pinned and clamped-sliding) and found that the effects of end conditions on the natural frequency is limited up to the first few modes of vibration only, and suggested the empirical methods for finding the natural frequencies of vibration in the higher modes. For a highly tensioned beam, depending upon its length/area of the cross ration (i.e., if it is too large), the natural frequency is independent of the flexural rigidity, and beam behaves like string. Howells (1995) showed that the SCRs are suitable for the deep water drilling and production and the use of various layers of different materials around the marine riser make it suitable for application to the 'High Pressure and High Temperature (HPHT)' conditions. These layers are arranged and knotted to ensure superior performance. Watters *et al.* (1998) reported a study on the performance analysis of marine riser with various current-based loading conditions, and they implied that the effect of current is on the natural period of riser motion. Also, they noted that in the absence of current, the natural period of riser motion is very high compared to that of current. Campbell (1999) presented the fatigue analysis of marine risers under the TDA and FDA's higher and lower frequency motions with their limitations explained in detail. He identified the critical locations that are sensitive to fatigue damage. The connection point of the marine riser to the floater and the 'Touch Down Point (TDP)' are found to be highly sensitive to the fatigue damage.

Vikestad *et al*. (2000) studied the vibration of marine risers under the effects of sheared flow by using the energy balance model. The different oscillating frequency at different locations along the length of the marine riser was observed due to the sheared current velocity profile. The damping model based on the existing riser response was constructed and found that the damping force is a function of reduced velocity and the non-dimensional parameter - A/D, where the A is vibration amplitude, and the D is cylinder diameter. Mekha (2001) reported a study on the fatigue aspect of marine risers and observed that the fatigue damage is sensitive to the offshore platform motion and VIV. He also identified the areas like the TDP and floater connection points where the fatigue damage is more likely to happen. Roveri and Vandiver (2001) discussed a parametric study of the fatigue damage under an action of the current velocity and the top tension in FD by using the Shear7*****TM software solution system. They observed that the current profile with compared to that due to the a low probability of occurrence produces some significant fatigue damages compared to that of the current profile with a high probability of occurrence.

Jauvits and Williamson (2004) presented an oscillatory model of the SCR that analyses the structural vibration motions in both directions, i.e., in-line to the flow and cross-flow (i.e., perpendicular) direction. They observed that, the in-line and cross-flow motions are related to each other under certain conditions, e.g., for the mass ratio > 6. The static and dynamic behavior of marine risers was studied by (Ljustina *et al.* 2004), and they considered motions in different directions.

Huarte *et al.* (2006) presented a study on the time-dependent fluid force distribution on the flexible marine riser with initial tension by using an indirect FEM in the presence of steeped current. Their results showed that the drag coefficient follows the pattern of RMS value of the CF motion of the marine riser (i.e., cylinder).

Vandiver *et al.* (2006) investigated the fatigue damage of marine risers at higher mode numbers (i.e., >10) in both uniform flow and sheared flow, and he observed that the contribution of higher modes in fatigue damage is very significant. The fatigue damage due to all the harmonics up to three is almost 40% more than that due to only the lower natural mode. Serious fatigue damage in the higher modes can be because of the narrow band of reduced velocity. Miliou *et al.* (2007) analyzed the flow past quarter segment of a solid ring to study the wake dynamics of flow at Re of 500 and

observed that the orientation of stagnation face with the free stream direction governs the three-dimensional flow pattern past the quarter of ring, and it almost behaves like a bluff body because of the low Re.

Modarres-Sadeghi *et al.* (2010) studied the higher harmonic response of a deep-water marine riser to find the effect of harmonic forces on the fatigue life of marine risers. They observed a significant contribution of the third harmonic in the fatigue damage, and also the fifth harmonic response was also observed being significant sometimes. They used the RRM to find the data at points where sensors were not installed. Their studies reinforce the importance of the lower odd number of modes, i.e., 1, 3, and 5. In the code - DNV-OS-F201 (2010) - it has been suggested that most of the earlier studies on the fatigue damage of marine risers due to VIV were based on the time-dependent lift forces acting in the transverse directions. Although the marine riser is expected to vibrate in the IL motion at low even modes (i.e., 2/4/6) with lesser amplitude in comparison of vibration in the CF motion at high odd modes (i.e., 1/3/5/7/9/11) with higher amplitude, the amplitudes are still significant in IL motion, and these amplitudes contribute to the fatigue because they are expected to have higher frequencies. Because of these reasons, it has been observed that the fatigue damage due to the IL motion of the riser contributes significantly and cannot be neglected. Hence, it is important to explore, investigate, and integrate the strong coupling between the IL and CF motions with the fatigue damage analysis. If the amplitude of CF vibration is of the order of magnitude of one diameter, then fatigue damage due to IL motion is around 30% - 50% of that due to the CF.

Khan *et al.* (2011) studied the dynamic response of marine risers under the regular and random waves, with and without current velocity. When the marine riser is subjected to only the random waves and the random waves with current, some significant changes in the response characteristics were observed, and these changes are due to the presence of higher harmonics because of the current velocity. Their results again show the strong dependence of the response of the marine riser on the current velocity. Srinil (2011) presented a study on the motion analysis of marine riser based on the dynamically varying tension, and in his model, the governing partial differential equations of the marine riser are the same as that of a tensioned vibrating string with the pinned-pinned end condition. His proposed model was able to predict the CF motion of marine riser in linearly sheared current, and he observed that in the gradual variation of the current velocity, the marine riser exhibits characteristics of the standing waves at mid-span of the marine riser and the combination of standing and traveling waves at the spans due to the multimodal frequency responses and their interferences.

Wu *et al.* (2012) discussed various aspects of the VIV characteristics on some higher and lower aspect ratio (i.e., length/diameter) structures, and in their study, huge differences were observed in the motion characteristics. The motion under lock-in conditions was not uni-modular, and it was multi-modular. The wave propagation along the length of the marine riser showed the traveling wave nature and the traveling wave coincided with the reflecting waves from the end and produced the standing waves somewhere along the length of the marine riser. For the low aspect ratio structures, the IL VIV, higher harmonics, lift force and standing waves have lesser effects on the VIV characteristics of the marine riser. Morooka and Tsukada (2013) discussed the dynamic responses of the marine riser with a scale factor of 250 in the towing tank, with the Re varying from 400 to 600. Their results showed that the CF responses of marine riser strongly influenced the traveling waves. Rivero-Angeles *et al.* (2013) presented a study on the model parameters of marine risers (i.e., the natural frequencies and mode shapes) to understand the dynamic behavior of long and slender marine risers using the theory of free vibration. They observed that the model parameters are affected

by the acceleration only data and natural frequencies and mode shapes are independent of end boundary conditions for the long and slender marine risers. Wang *et al.* (2013) identified the influence of sea bed stiffness on the fatigue life of marine riser by using the linear hysteric loop and they observed that if the sea bed stiffness increases, the fatigue life of marine riser will decrease.

They also suggested that the soil parameters like shear strength of mud line, soil suction, and TDP strongly influence the marine riser fatigue life. Chen *et al.* (2014) studied the effects of a floater heave motion on the deep water marine riser and its coupling with the VIV motion. They observed that the VIV response of marine riser is significantly high with the top heave motion compared to that without the heave motion. Also, they noted that the standing waves dominate the lower mode responses, and the traveling waves dominate the higher mode responses of the marine riser. Although, the 'Finite Element Method (FEM)' based computation of the marine riser fatigue with higher modes is a known approach among researchers, in best of our knowledge and understanding these do not consider the marine riser and offshore platform together in to the analysis. Usually, if the FEM approach is used then the platform motion is consider in only one direction by the researchers, e.g. heave in Chen *et al.* (2014). Furthermore, the magnitude of displacement motion increases linearly with an increase in the tension at the top of the marine riser. Lei *et al.* (2014) reported an FDA to identify the effects of timevarying axial tension on the deep water marine riser due to heave motion of the floater by modeling the marine riser as the 'Euler-Bernoulli (EB)' beam. Their presented model can compute the dynamic responses of marine riser under the combined effects of random waves and the top end heave parametric excitation. They also observed that the heave motion frequency and amplitude have a more significant influence on the dynamic response of marine riser than that due to the motion in other DOFs. Xue *et al.* (2014) presented a numerical model based on the 'Energy Equilibrium Method (EEM)' to simultaneously study the IL and CF VIV motions induced fatigue damage of the marine riser. They noted that IL motions' amplitudes are smaller than the CF motions. However, the maximum fatigue damage due to both the IL and CF motions are significant because the IL motions are of low amplitude and high frequency and the CF motions are of high amplitude and low frequency. Also, they observed that the fatigue damage is highly sensitive to the surface current velocity. The 'present study has reinforced these observations'.

2.1 Important limitations of the existing literature

From the brief review of literature, we note the following limitations:

- (A) It is well known that the VIV is a major source of fatigue damage in deep water marine riser due to its oscillating nature and even though the amplitudes of vibration are small, the higher frequency VIV dominates in fatigue damage analysis. Almost all the existing studies on the fatigue damage analysis of marine risers are based upon either the CFD-based software solution systems or experimental analyses. The experimental studies are expensive and complex in their setup. Also data acquisition from experiments is difficult as it requires large numbers of instruments which is very difficult to fabricate in real structure, e.g., in the current problem marine structure's length and operating depths are very high, 1200 m length and water depth 1000 m and they are very difficult to achieve in the laboratory setting even with a high scaling. Hence, we believe that the design and development of a CSM that can reflect the real-time situations of deep water marine risers with minimum possible cost and complexity is an economic, efficient, highly applicable, and appropriate option.

-(B) In general, the CFD methods are prevalent for problems of lesser sizes. However, these methods are time-consumingthese methods are time-consuming for the real marine structures and demand a huge considerable memory for the real marine structures. In most of the existing literature, the fatigue damage of marine has been reported by considering the marine riser as a sole component or by modeling the marine riser floater system through parametric excitation. The marine risers are always attached to an offshore platform at top end via a flexible joint in the real world. So, the motion of an offshore platform (i.e. semi-submersible in the present study) in all the six DOFs is transferred to the marine riser along its length in form of the travelling waves.

- (C) Also, to save computation time most of the existing studies have been reported in the FDA where all the modes of vibrations are not taken into consideration. A neglect of the higher modes is likely to underpredict the fatigue damage.

- (D) As far as the dynamic analysis and the subsequent prediction of fatigue damage are concerned, there exist some important limitations in the existing literature, e.g.

- Only the lower mode vibrations (i.e., first and second) are studied while ignoring the higher modes.
- Only the bare marine riser is considered while ignoring the coupled motion analysis because of the presence of offshore platform. And, even when the offshore platform's motion is considered it is considered as a single DOF input. And, only a specific type of the current profile is considered while ignoring the others.

This work addresses the limitations as mentioned above. Herein, the advantages of time domain and frequency domain are incorporated to obtain an efficient computational modal for the fatigue damage analysis applied to the deep water marine risers. The semi-submersible motions are computed in the FDA as the RAOs, and they are imported to the TDA for the marine riser's fatigue analysis. Using some suitable transfer functions, the RAOs of semi-submersible are converted into the motion time histories and used as the top end boundary conditions in the marine riser' dynamic analysis. Details of analysis have been reported earlier in Fig. 2.

2.2 Research contribution

We present the design and development of a CSM for the fatigue damage analysis of deep water marine riser with and without VIV under the influence of waves resulting from the sea states of 4 to 9. The proposed CSM is presented with detailed results under two case studies: Comparison of the fatigue damage with and without the VIV in the presence of coupled offshore platform motion analysis, and Comparison of the fatigue damage with two different current profiles (i.e., linear and power laws). Additionally, the presented results are analysed in detail under the underlying physics and utilized to extract simple, implementable, and highly relevant design guidelines applicable in the preliminary design stages of offshore platform and marine riser.

3. Basic mathematical preliminaries

We consider various forces acting on the marine structure (i.e., marine riser) and the responses of riser and offshore platform (i.e., semisubmersible) are computed with the developed numerical

model. As the main source of fatigue damage is the current velocity and VIV, we focus in-detail on the modeling of VIV forces and nature of current profile and use them in the numerical mode. We use the fundamentals from theory of vibration, fluid mechanics, marine hydrodynamics and numerical analysis, i.e., Blevins (2001), Dahlquist and Björck (2003), Thomson (2004), Naudascher and Rockwell (2005), White (2015), Cengel and Cimbala (2017), and Newman (2018).

3.1 Frequency domain analysis (FDA)

A brief description about the FDA and its application is shown in Fig. 3. In the FDA the geometric parameters of the semisubmersible are given as an input and the 'Response Amplitude Operators (RAOs)' are the output. Then these RAOs are the input in 'Time Domain Analysis (TDA)'. In the FDA we focus on the radiation and diffraction forces and utilize them to analyze offshore platform (i.e., semi-submersible in the present work) to compute the RAOs. The radiation force is due to the motion of semi-submersible in still water and the radiated wave field computes it. The wave excitation force is composed of diffraction due to scattering of incident wave and the 'Froude-Krylov (FK)' forces due to the differential pressure distribution around body.

We assume that the incident and radiation are both harmonic, fluid is ideal, incompressible, irrotational, and hence the potential flow solution is used. In the numerical solution, the fluid singularities are distributed over the wetted surface of floating body.

- *(A) Basic stability analysis in the FDA:* Following TMAA (2014), the basic equilibrium analysis of semi-submersible is done by eliminating the out-balance forces and moments and in reference to Figs. 4 and 5 this implies the following

$$\mathrm{F}_{Hys} = \int_{\mathrm{s}} p\,\hat{n}\,\mathrm{ds} \tag{1}$$

$$M_{Hys} = \int_{\mathrm{s}} \mathrm{p}\,\left(\vec{r}\times\vec{n}\right)\mathrm{ds} \tag{2}$$

where p is the pressure distribution, $\vec{n}$ is the surface unit normal, ds is the small element of surface, r is the distance from center of structure, F_{Hys} is the hydrostatic force and M_{Hys} is the hydrostatic moment. To achieve an equilibrium position of the offshore platform like semi-submersible, first of all we define the origin at center of gravity (CoG)) and global axis as $\mathrm{X_G}$, $\mathrm{Y_G}$ and $\mathrm{Z_G}$. By considering stiffness matrix in nonlinear form, equilibrium position of the semi-submersible is achieved numerically by considering simple stiffness and displacement relation (Hook's law). During each numerical iteration, stiffness matrix is updated to nullify the out balance forces. Let, the initial guess of structure's position and orientation be a vector X^0, where $X^0 = \{x_1, y_1, z_1, p_1, q_1, r_1, x_2, y_2, z_2 \ldots\ldots\}$ and (p,q,r) are the finite angular rotation, by using hooks law, displacement at each iteration is computed by using following Eq. (3)

$$\begin{aligned} dX^{(1)} &= K_h^{-1}(X^{(0)})F_k(X^{(0)}) \\ F_k &= B_{CG} - M(s)\,g \end{aligned} \tag{3}$$

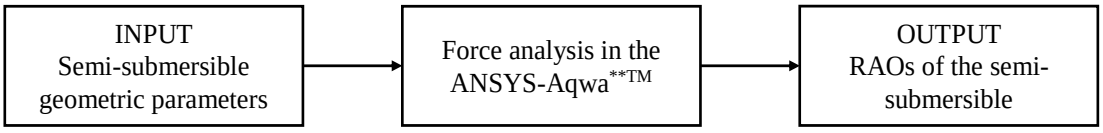

Fig. 3 Brief description about the FDA and its application

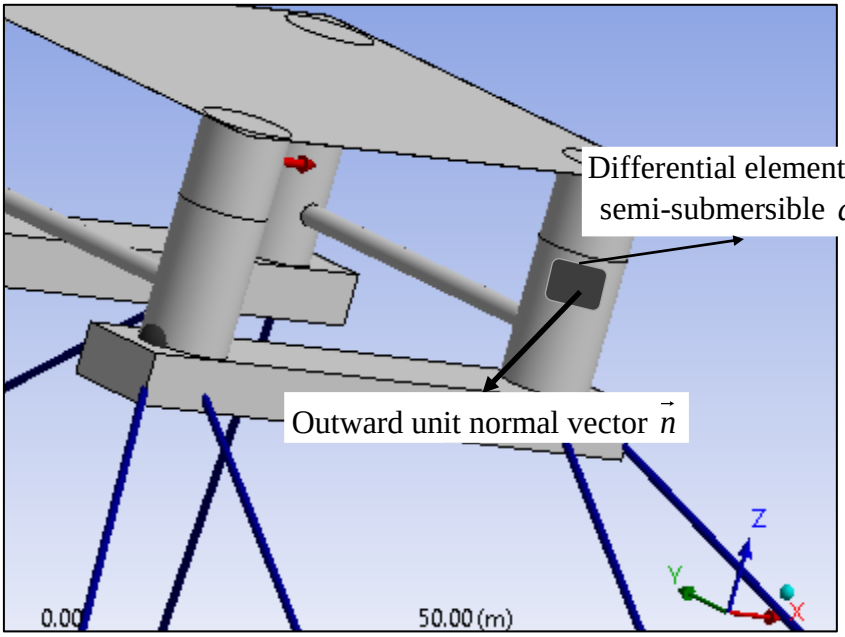

Fig. 4 Basic schematic and conventions of the stability analysis

where B_{CG} is buoyancy at the CoG, $M(s)$ is the mass of structure, g is the acceleration due to gravity and K_h is equal to $\rho g A_w$ where A_w is the water plane area.

The new position of body $X^{(1)}$ is:

$$X^{(1)} = dX^{(1)} + X^{(0)},$$

with convergence criteria: $dX \le dX_{\text{Prescribed}}$.

- *(B) Diffraction analysis in the FDA:* After the basic stability analysis of semisubmersible, the diffraction analysis is done to compute the RAOs. The hydrodynamic forces on semisubmersible are computed by finding the velocity potential for incident wave and the pressure distribution on structure. The velocity potential for flow field is computed by solving the following Laplace equation

$$\frac{\partial^2 \Phi}{\partial^2 x} + \frac{\partial^2 \Phi}{\partial^2 y} + \frac{\partial^2 \Phi}{\partial^2 z} \tag{4}$$

$$\Phi = \Phi_i + \Phi_s + \Phi_j$$

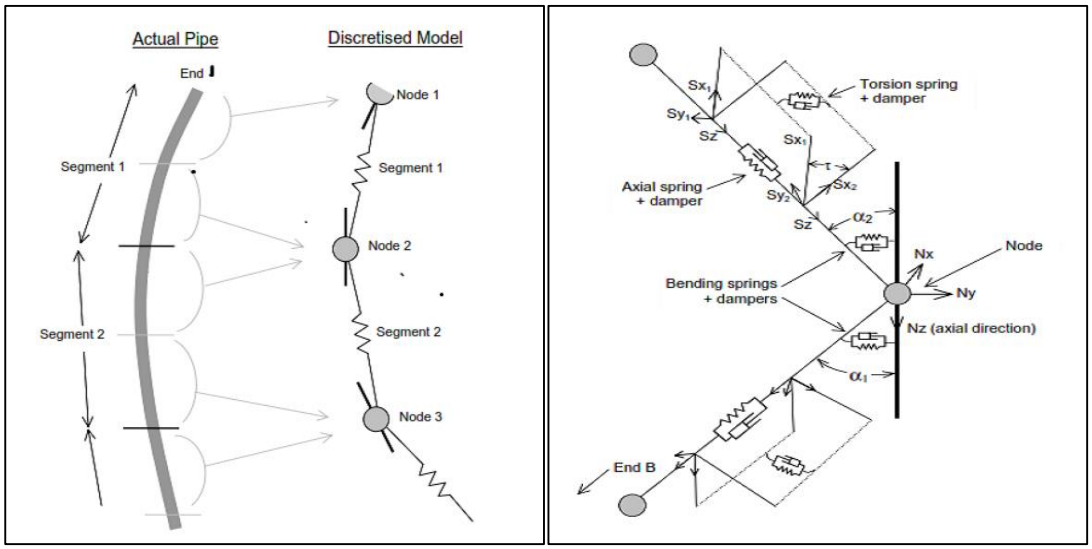

(a) Riser discretization (b) Riser element modeling

Fig. 5 Modeling of riser in time domain adapted from TMO (2013)

and it is subjected to the following boundary conditions

$$\left\{\begin{array}{l} \dfrac{\partial \Phi}{\partial y} = 0 \text{ at } y = -d, \ \dfrac{\partial \Phi}{\partial n} = \mathrm{V}_n \\ \dfrac{\partial \Phi}{\partial t} + \dfrac{\partial \Phi}{\partial x} * \dfrac{\partial \eta}{\partial x} + \dfrac{\partial \Phi}{\partial z} * \dfrac{\partial \eta}{\partial z} \\ -\dfrac{\partial \Phi}{\partial y} = 0, \text{ at y=} \eta \end{array}\right\} \tag{5}$$

$$\frac{\partial \Phi}{\partial t} = \frac{1}{2} * \left[\left(\frac{\partial \Phi}{\partial x} \right)^2 + \left(\frac{\partial \Phi}{\partial y} \right)^2 + \left(\frac{\partial \Phi}{\partial z} \right)^2 \right] + g * \eta, \text{ at y=} \eta \tag{6}$$

$$\frac{\partial \Phi_i}{\partial n} = -\frac{\partial \Phi_s}{\partial n}, \text{ -d} \le \text{y} \le \eta \tag{7}$$

$$\lim_{R \to \infty} \sqrt{R} \left(\frac{\partial}{\partial R} \pm i\lambda \right) . \Phi_s = 0 \tag{8}$$

where Φ is total flow potential, Φ_s is the scattered wave potential, Φ_i is the incident wave potential, Φ_j is the radiated wave potential, λ is the eigen value, d is the water depth, $\mathrm{V_n}$ is the velocity normal to surface, η is the instantaneous wave surface elevation and g is the acceleration

due to gravity. The total potential is the summation of diffracted wave or scattered wave potential, incident wave potential and radiated potential. An additional boundary condition is that at the infinity the scattered potential Φ_s needs to vanish at a great distance from the surface, e.g., at the distance R from the center of the structure and this results into Eq.(8).

Solution of Eq. (4) is given by the following

$$\Phi(\mathrm{x,y,z,t}) = \phi(\mathrm{x,y,x}) \times \exp(-\mathrm{i}\omega \mathrm{t}) \tag{9}$$

Now, with this Equation (9) is re-written as the following

$$\phi(\mathrm{x,y,x}) \times \exp(-\mathrm{i}\omega \mathrm{t}) = \left(\sum_{j=1}^{6} \phi_j x_j + \phi_i + \phi_d\right) \times \exp(-\mathrm{i}\omega \mathrm{t}) \tag{10}$$

$$\phi_i = \frac{-i\ g \cosh\ [\mathrm{k(d+z)}]}{\omega\ \cosh(\mathrm{kd})} \times \exp\ [i\,\mathrm{k}\ (\mathrm{x}\ \cos\theta + \mathrm{y}\ \sin\theta)] \tag{11}$$

where ϕ is the spatial flow potential, ϕ_s is the scattered wave potential, ϕ_i is the incident wave potential, ϕ_j is the radiated potential due to motion in the jth degree of freedom (x_j) and ω is the circular frequency. All these wave potentials are computed at the selected discrete number of points on the wetted surface of structure using the 'Greens integral' theorem along with the free surface boundary conditions. Once these potentials are computed, the pressure distribution over wetted surface is computed by a simple pressure potential relation and this implies the following

$$\mathrm{p} = -\rho \frac{\partial \phi}{\partial t} \tag{12}$$

where p is the pressure distribution and ρ is the sea water density. From the available pressure distribution, the excitation force in jth direction can be found by using the surface integration technique as mentioned in Eqs. (13) and (14), i.e.

$$F_j = -\int_s \mathrm{p}\ \mathrm{n_j}\ \mathrm{ds} = -\int_s i\omega\ \rho\ (\phi_i + \phi_d)\ \mathrm{n_j}\ \mathrm{ds} \tag{13}$$

$$F_j = -\int_s i\omega\ \rho\ \phi_i\ n_j\ \mathrm{ds}\ \ -\int_s i\omega\ \rho\ \phi_d\ n_j\ \mathrm{ds} \tag{14}$$

where F_j is the force in jth direction, n_j is the normal vector to jth element and the other terms are as defined before. First term of Eq. (14) implies the 'Froud-Krylov (FK)' forces and the second term implies the diffraction forces. Radiation forces acting on body are computed by the following

$$F_{ji} = -\int_s i\ \omega\ \rho\ \phi_j\ x_j n_j\ \mathrm{ds} \tag{15}$$

where F_{ji} is the force in ith direction due to motion in jth degree of freedom. Once the fluid forces are modeled on semisubmersible, the RAOs are computed by solving linear second order differential

equation and this can result into the following

$$M(s)\ \frac{d^2X}{dt^2} + M(a)\ \frac{d^2X}{dt^2} + c\ \frac{dX}{dt} + k_s\ X = F(t) \tag{16}$$

where M (s) is mass of semisubmersible, M (a) is the hydrodynamic added mass matrix of semisubmersible, c is the system linear damping matrix, k_s is the total stiffness matrix of the semisubmersible, X is the RAO of semisubmersible and F (t) is the external excitation force.

- *(C) Discretization and modeling of riser in the time domain:* The analysis of marine riser is done in the non-linear time domain and it is implemented in the OrcaFlex*TM. We use the finite element analysis based approach and each of the elements of riser is modeled as a damped spring mass system, i.e., spring mass and damping as shown in Figs. 5 (A) and 5(B). The elements are arranged in a series and the structural boundary conditions at the ends are matched to ensure a continuous solution.

- *(D) Modeling the ocean environment:* Normally, the buoyancy of a floating object is assumed to be constant and often neglected for its variation along the water depth. In practice this is not strictly true, e.g. the buoyancy of an object can change because of the following:

I. Use of inflatable/deflatbale materials results in the change of volume, which implies the change in buoyancy. The forces of compression and tension can cause contraction and expansion, thereby changing the volume and resulting in buoyancy changes.

II. Sea water density changes across the ocean water depths and it is a function of different parameters, e.g. temperature, pressure and chemical composition, etc. Therefore, the riser and the attached elements undergo the buoyancy changes, which is considered in the present work. The horizontal current profile is specified in the full 3D profile and it is a variable both in the magnitude and direction along the water depth. The current velocity at the surface and bottom is specified along with the nature of current profile and its variation with the mathematical equation.

Herein, we consider two variations in the current profile: Linear variation and power law (1/7) variation. Herein, we consider the random waves and Random waves can be modeled as frequency wave spectra like JONSWAP, ISSC, and Ochi-Hubble, etc. The phase associated with each of the wave components is random and a random number generator is used to assign a random phase. In present study we have considered JONSWAP wave spectrum as discussed below.

The VIV is a current dominated phenomenon and the waves have a strong tendency to excite the forces and get coupled with the current. The wave forces dominate the North sea and the current speed in the North sea typically varies from 0.6 to 1.0 m/s and higher with sea states varying from 6-8, significant wave heights varying from 4 to 14 m, sea characteristics varying from very rough to very high and sea swell varying from the short to long, for more details see (Danielssen *et al.* 1997). For the North Sea the JONSWAP spectrum was developed for limited fetch (i.e., it is the distance from a lee shore or the distance over which the wind blows with constant velocity) and because of this we use the JONSWAP spectrum, for more details see Hasselmann (1966) and Hasselmann *et al.* (1973).

- *(E) Construction of wave components:* Following Techet (2005) and TMO (2013), an irregular wave is generated by the linear super position of regular waves and for the JONSWAP spectrum it is defined as the following

$$\left\{\begin{array}{l} S^{+}(w)=\dfrac{\alpha\, g^{2}}{w^{5}}\ \exp\left(\left\{-1.25\,\gamma^{\delta}\left(\dfrac{w_m}{w}\right)^{4}\right\}\right) \\ \alpha = 0.076\,\bar{x}^{(-0.22)},\ \bar{x}=\dfrac{g\,x_s}{u_s^{\,2}},\ \delta=\dfrac{(w-w_m)}{2\,\sigma^{2}\,w_m^{\,2}} \\ \sigma=\left\{\begin{array}{l} 0.07,\ \text{if } w \le w_m \\ 0.09,\ \text{if } w > w_m \end{array}\right\} \end{array}\right\} \tag{17}$$

where $S^{+}(w)$ is the frequency dependent spectral energy, α is a constant depending upon the wind velocity, g is the acceleration due to gravity, γ is the shape factor of spectrum, w is the angular frequency, w_m is the peak spectral frequency, x_s is the fetch distance and u_s is the wind speed at 10 m above sea surface. We consider the following:

- Overall frequency range is from $0.5*f_m$ to $10*f_m$ where f_m is the maximum frequency and the spectral energy outside this range is neglected. We use the standard enhancement parameter value of 3.3 as suggested by Hasselmann *et al.* (1973).

- Overall frequency range is discretized into the n components, i.e. f_{i-} and f_{i+} at the end frequency content in the random wave is equal to the sum of energy contained by regular waves.

3.2 Modeling of the loads on marine riser

- *(A) Tension load:* Following Faltinsen (1993) and TMO (2013), the tension at centre of each line segment is computed by the following vector equation

$$\begin{aligned} T_e = {} & E\,A\,\varepsilon + (1-2\,\upsilon)\,(p_0\,A_0 - p_i\,A_i) \\ & + E\,A\,e\left(\frac{dL}{dt}\right)_{L_0} \end{aligned} \tag{18}$$

where T_e is the effective tension, EA is the axial stiffness, ε is the axial strain, L is the length of segment, L_0 is the un-stretched length, υ is the Poisson ratio, p_i and p_0 are the internal and external pressures respectively, A_i and A_0 are the internal and external areas respectively, e is the damping co-efficient in the tension, and dL/dt is the rate of change of length with respect to time. The 'e' is e (critical) * (target axial damping)/100, and the e (critical) is defined as the following

$$e(critical)=\sqrt{\frac{2.(\text{mass}).L_0}{EA}} \tag{19}$$

where 'mass' is the mass of a particular element being considered in the marine riser and the other terms are as defined before.

- *(B) Bending load:* Following Faltinsen (1993) and TMO (2013), the bending load on marine riser in the TD is given by the following

$$M=E\,I\,|C| + D\left(\frac{d\,|C|}{dt}\right) \tag{20}$$

where EI is the bending stiffness of marine riser, $D = D_c\ (\lambda_t/100)$, D_c is the critical damping for bending, λ_t is the target bending damping and C is the curvature of marine riser.

- *(C) Shear force:* Following Faltinsen (1993) and TMO (2013), each of the segmental lengths of marine riser is considered as a stiff straight rod and bending moment at the end of each element is M_1 and M_2, then the shear force at each element is given by the following

$$\text{S.F. (Shear force)} = \frac{M_2 - M_1}{L} \tag{21}$$

where L is the elemental length and other terms are as defined before.

- *(D) Torsion moments:* Following Faltinsen (1993) and TMO (2013), the torque on marine riser in the TD is given by the following

$$\text{Torque} = \frac{k_t\ \tau}{L_0} + C_t\ \left(d\tau/dt\right) \tag{22}$$

where k_t is the torsional stiffness, τ is the segmental twist angle, L_0 is the un-stretched length of marine riser, $\left(d\tau/dt\right)$ is the rate of change of twist w.r.t. time and C_t is the torsional damping coefficient.

- *(E) Background of the VIV and modelling: The VIV is a complex phenomenon for viscous fluid flow* over the bluff bodies. As a flow progresses on bluff body - from low Re to high Re - the viscosity effects starts dominating, i.e., retardation of the boundary layer formed on it. This retarded boundary layer is no longer capable of moving further in downstream from a certain point and this causes the flow to get detached from the body surface, i.e., flow separation. The flow separation creates a low pressure region downstream of bluff body in-side the wake region. The difference between the upstream and downstream fluid pressures causes the body to oscillate and accordingly the wake behind bluff body also oscillates. This oscillation of the wake region is called the VIV, e.g., well known example is the formation of vortices. In the potential theory the forces associated with the flow separation cannot be incorporated and because of this the VIV loads are modeled in the TD. Herein, we use the 'Wake Oscillator Model (WOM)' of Iwan and Blevins (1974). The WOM uses a single dof model to represent the wake generated behind a rigid cylinder and oscillation is considered the function of time. The oscillation of wake generates a lift force on the cylinder, i.e. normal to the cylinder axis and flow direction. The WOM uses the single dof to compute the lift force and the motion of cylinder changes the VIV characteristics. This induces the feedback motion of cylinder and that in-turn changes the dynamic characteristics of cylinder motion. All the line elements of riser undergo this kind of feedback motion, and each element's time history is recorded. The detailed equation of motion of wake and its solution procedure through a semi-empirical approach have been studied in Iwan and Blevins (1974) and the same is used in this work.

- *(F) Total loads on marine riser:* All the above mentioned loads and moments from Equations (18-22) are experienced by each of the elements of riser at either side. These loads are added up to other non-structural loads and moments to compute the total loads on marine riser. After the computation of total load only the first phase of TD simulation starts. The first step in TD simulation is the static analysis of combined floater and marine riser system to achieve its equilibrium position.

However, herein, in the present CSM we do not focus on computing the individual Froude Krilov, radiation and diffraction component for the marine riser. Since, the marine riser fatigue problem is

predominantly based on the current and VIV, therefore the diffraction analysis has not been the focus for marine riser. However, the semi-submersible diffraction analysis has been done to compute its RAOs.

3.3 Static analysis

Static analysis of combined floater and marine riser system is aimed for: To achieve the equilibrium position under the actions of buoyancy, and hydrostatic and hydrodynamic pressure distributions across the depth, etc. The initial position of marine riser and the platform is specified by the user with some approximation and then the out of balance force method is used to identify the system's equilibrium position iteratively. During each time step of the static analysis the out of balance force is computed and correspondingly a new position is specified. These iterations continue till the out of balance force becomes zero. The system position at which the total out of balance force is zero is the system's static equilibrium position.

- *(A) Modal analysis:* The un-damped natural frequencies and periods are computed using the modal analysis methods and we consider three types of modes: in line, cross flow and axial modes. Their contribution is computed in % terms. Following Thomson (2004) and TMO (2013), the governing equations for modal analysis are the following

$$M(r)\, a_r = -k_r\, p_r \tag{23}$$

$$p_r = A \sin(\omega_{nr} t) \tag{24}$$

where p_r, and a_r are the position, and acceleration at any specify time t on the marine riser element, M_r is the mass matrix of marine riser element (including the added mass), k_r is the marine riser element stiffness matrix, A is the amplitude of motion of the marine riser and $\omega_{nr} = \sqrt{\frac{k_r}{M_r}}$ is the natural circular frequency of marine riser.

3.4 Dynamic analysis

A dynamic simulation is the analysis of marine riser floater combined system under the offshore platform motions that are because of ocean environmental loads and the feedback structural loads from the marine riser to floater motion. The dynamic simulation starts at the end of static simulation and the period of entire dynamic simulation is divided into different time stages as per the requirement to provide smooth start of the simulation. The first stage of simulation is the build-up stage, during which the ocean wave, vessel motion, and current smoothly ramped up from the zero to their full developed values. The different time segments of dynamic simulations are shown in Fig. 6.

- *(A) Computational method of dynamic analysis:* We use the linear second order ordinary differential equation of motion and solve it numerically to compute the response and load time history on each of the elements of marine riser. Following Thomson (2004), TMO (2013) and Newman (2018), the governing equation of motion is the following

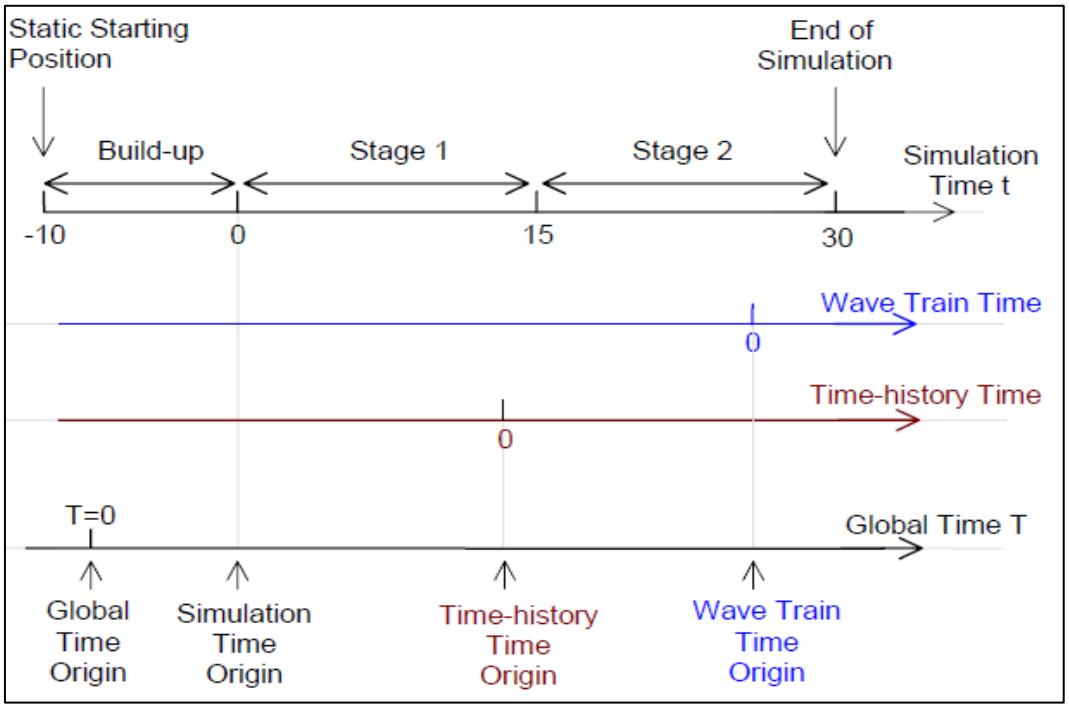

Fig. 6 Different time segments of the dynamic simulations adapted from TMO (2013)

$$M_r(p_r, a_r) + C_r(p_r, v_r) + k_r(p_r) = F(p_r, v_r, t) \tag{25}$$

where $M_r(p_r, a_r)$ is the marine riser's inertia load (including added mass), $C_r(p_r, v_r)$ is the marine riser damping load, $k_r(p_r)$ is the riser stiffness load, p_r, v_r and a_r are the position, velocity and acceleration at any specify time t on the marine riser element. The solution of Eq. (25) is computed using a numerical integration scheme, i.e., explicit integral scheme, for more details see Dahlquist and Björck (2003).

- *(B) Explicit integral scheme for solution of Eq. (25):* Following, Dahlquist and Björck (2003) an explicit integral scheme is a forward difference Euler integral scheme with constant time steps and utilizing this Eq. (25) is solved for the velocity at each of the time steps for each element. This implies the following

$$(v_r)_{t+1} = (v_r)_t + dt.(a_r)_t \tag{26}$$

where the terms are as defined previously. This velocity is integrated by the same scheme to compute the position of each of the elements and it results into the following:

$$(p_r)_{t+1} = (p_r)_t + dt.(v_r)_t \tag{27}$$

where the terms are as defined previously.

A proper time step is required for the stable integration and its choice is important because a lower time step results into better convergence with high computational time and a higher time step

results into poor convergence with low computational time. Hence, a compromise is sought. As a simple rule a time step is normally 1/5000 to 1/10000 of the time duration in which the steady state is expected to reach and for the sake of lower computational cost a higher value is chosen, i.e. 1/5000 of time duration. Although, our time duration is 1000 s, we also reach the steady state response at around 100 s. Hence, we use a time step of 100/5000 = 0.02 s. Therefore we use a time step of 0.02 seconds.

3.5 Fatigue analysis

Essentially, in the fatigue, a structure fails at lower stress levels than the yield stresses and this failure of the material is due to the cyclic loading effects. As far as the load's amplitude and number of cycles (N) are concerned there exist four combinations: load with high number of cycles and low amplitude; load with low number of cycles and high amplitude; load with low number of cycles and low amplitude; and load with high number of cycles and high amplitude. Although, the fatigue related behavior has randomness, out of these parameters the fatigue is affected by the number of cycles more and lesser by the load amplitude (i.e., above the endurance limit only). Below this endurance limit load a material will not fail even with abnormally high number of cycles, for more details see Beer *et al.* (2016). A crack may result because of the fatigue related failure and its propagation will be affected largely by the number of cycles and tensile loads rather than its amplitude and compressive loads. Normally, the fatigue failure starts with a crack and then this crack widens with the gradual enlargement and propagates further during different loading cycles. Since, the fatigue failure is due to cyclic loading, the parameters like number, duration and magnitude of the loading cycles are utilized in the analysis.

Following Lieurade (1989) and TMO (2013), we consider a time dependent cyclic stress and apply that to an element with $\sigma_{\max}$ and $\sigma_{\min}$ being the maximum and minimum stress amplitudes and with these the differential stress amplitude σ_a and mean stress σ_m are defined as the following

$$\sigma_a = \frac{\sigma_{\max} - \sigma_{\min}}{2}, \text{ and } \sigma_m = \frac{\sigma_{\max} + \sigma_{\min}}{2} \tag{28}$$

Fatigue failure analysis is done by counting the number of load cycles, magnitude of the load and sign of the load that are required to cause failure. All of these are directly related to the ranges of stress amplitude. The quantitative description of relation between the range of stress amplitude and the number of cycles corresponding to that range of amplitude is given by the S-N curve. From the perspective of material science, the fatigue failure is the result of the accumulated stresses in the material and although individually these stresses are low their accumulation results into significantly higher values. The resultant stress becomes the instantaneous stress plus the accumulated stress and when this resultant stress exceeds the yield stress the material fails, for more details see Schijve (2009).

In the fatigue damage computation, we assume that each of the load cycles is producing an equal amount of the damage to the element during its life time. The load time history is obtained from the dynamic analysis of system and it is used to compute the range of stresses that are induced by these loads. Then by using the 'Rainflow Counting (RC)' method the numbers of load cycles are counted. Now, if we assume that the N_i is the number of the stress cycles of amplitude σ_{ai} undergone by an

element, then the fatigue life of that element is computed by using the linear cumulative fatigue damage approach. Following, Schijve (2009) this implies into the following

$$D_i = \frac{N_i}{N_{fi}} \tag{29}$$

where D_i is the 'Fatigue Damage Index (FDI)', N_i is the number of stress cycles, N_{fi} is the minimum number of stress cycles needed to cause failure under that class of load. The class of load includes the magnitude, and type, etc.

- *(A) S-N curve:* Most of the fatigue failure happens because of the large numbers of loading cycles regardless of their range of the stress amplitude. In-general, this implies that the fatigue failure is more dominated by the frequency rather than the amplitude. Some materials (e.g., ferrous alloys like steel) exhibits a stress level called endurance limit, below which the fatigue failure of an element will not happen. As the mean stress level affects the fatigue strength, a higher mean stress results in smaller cycles needed to cause fatigue failure. On the log-log scale the S-N curve can be approximated by a straight line as shown in Fig. 7, and the power law relation is used and this is the following

$$N_1 = N_2 * \left(\frac{S_1}{S_2} \right)^{1/b} \tag{30}$$

where b is the slope of S-N curve N_1 and N_2 are the load cycles corresponding to the S_1 and S_2 stress level.

- *(B) Rainflow counting method:* In the narrowband time series, the individual stress cycles can be easily counted by counting one stress cycle for each zero crossings (with positive slope) and taking the stress range as the difference between peak and valley values. In the broadband time series, where many cycles are to be investigated with small cycles with varying mean levels, the stress range becomes less evident. Therefore, it is necessary to use the cycle counting methods that break the stress time history into the individual cycles which can be summed up into the stress range distribution. The rainflow starts at each of the peaks and troughs, when a rainflow path starts at the trough, comes to the tip of roof, then the flow stops if opposite trough is more negative than the one from where flow started initially. For the rainflow started from peak, it is stopped by the peak which is more positive than the one from where the flow started. We present an example below to show the process of rainflow counting, i.e., for a given broadband time history, the details are the following:

- (A) Trough generated half cycles: 1-8, 3-3a, 5-5a, 7-7a, 9-10, 11-12, and 13-14.
- (B) Peak generated half cycles: 2-3, 4-5, 6-7, 10-12b, 12-12b, and 8-9-13.
- (C) Total numbers of full cycles: 2-3-3a, 4-5-5a, 6-7-7a, 9-10-12b, and 11-12-12a. (D) Total number half cycles: 1-8, 8-13, and 13-14.

Above mentioned process of cycle (A-B-C-D) counting is used to identify the total numbers of half and full cycles of load from the stress time history generated at the end of dynamic simulations. The S-N curve is used along with the counted number of cycles to identify the stress amplitude associated with the fatigue failure corresponding to these numbers of cycles.

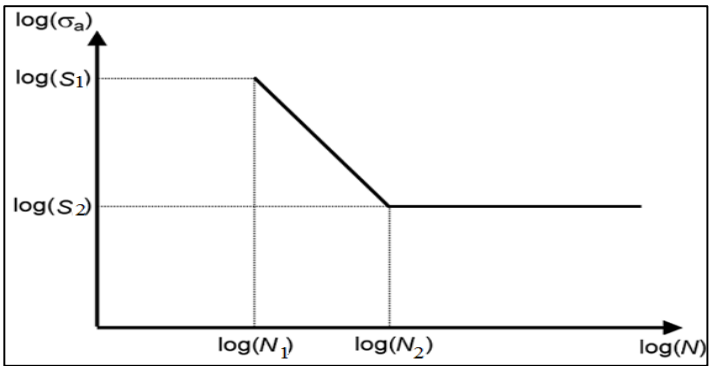

Fig. 7 A sample S-N curve for the fatigue analysis on the log-log scale, adapted from TMO (2013)

4. Computational model for modeling semisubmersible and riser in frequency domain and time domain respectively

Herein, the 'Computer Simulation Model (CSM)' for fatigue analysis of the marine riser along with the offshore platform is developed in an integrated and modular structure. The CSM consists of two sub-models and they are: Frequency Domain Computational Model (FDCM) and Time Domain Computational Model (TDCM). These models are further developed into different modules and only the geometric details module is common to the FDCM and TDCM. We focus on coupling the FDCM and TDCM to achieve better accuracy and higher computational efficiency. In-general the FDCM is computationally less demanding in comparison to the TDCM but it cannot compute the dynamical parameters efficiently and because of this a coupled analysis is helpful. In the FDCM, the important modules are:

- FDCM: Module 1 - This is common to the FDCM and TDCM and it deals with the geometric, material and other related parameters of the marine riser and offshore platform along with ocean environment parameters.
- FDCM: Module 2 - It deals with the FDA. The input here is from Module 1 and this module is implemented in the selected software, i.e., Ansys AQWA^{**TM}.
- FDCM: Module 3 - It deals with the discretization of the offshore platform (i.e. semi-submersible in this work). The discretization is important because the computational accuracy, convergence and efficiency depend upon the discretization. Herein, we focus on the numbers of elements/panels to be generated and the relevant boundary conditions that are imposed on the structure.
- FDCM: Module 4 - The floating structures are governed by the geometric forms and not to the limits of material characteristics and because of this the conditions related to stability and buoyancy, etc. gain critical importance. This module deals with the hydro-static/dynamic equilibrium analyses and results into the stable equilibrium positions for the offshore platform.
- FDCM: Module 5 - It deals with the diffraction analysis and it is used to compute the RAOs of offshore platform. These RAOs are used to determine the motion time history of offshore platform in Module 4 of the TDCM.

In the TDCM, the important modules are:

- TDCM: Module 1 - This is common to the FDCM and TDCM as mentioned before.

- TDCM: Module 2 - It deals with the finite element base computations in time domain. This is used for the dynamic analysis of marine riser and offshore platform as an integrated system. The input here is from Module 1 and this module is implemented in the selected software, i.e. OrcaFlex*TM.

- TDCM: Module 3 - It deals with the discretization of marine riser for the usages in finite element analysis with suitable boundary conditions.

- TDCM: Module 4 - It receives its input from Module 5 of the FDCM and these RAOs are utilized in the TDA after their conversion into the motion time histories by using transfer functions. Then the marine riser is connected to the offshore platform and the motion time histories of offshore platform are utilized in the imposition of top end boundary conditions on the marine riser. This imposition ensures end to end continuity, connection and integration of the marine riser with offshore platform.

- TDCM: Module 5 - It deals with the static equilibrium analysis for the marine riser and offshore platform as an integrated system and the output from here is utilized to initiate the dynamic simulation process of integrated system.

- TDCM: Module 6 - It deals with the dynamic analysis of integrated system.

- TDCM: Module 7 - It deals with the computations of structural loads on the marine riser, i.e. wave and current induced loads, tension, compression and torsion, etc. and the motion responses of riser under these loads, i.e. acceleration and velocity etc.

- TDCM: Module 8 - It deals with the rain-flow counting method that is used to compute the numbers of loading cycles.

- TDCM: Module 9 - It deals with the computation of 'Fatigue Damage Index (FDI)' and herein we utilize the S-N curve and the output from Module 8. The FDI is computed in a linear cumulative manner and is based upon the Miner's rule as mentioned previously in Chapter 3. The detailed modular structure of the proposed CSM for fatigue damage analysis has been already shown in Fig. 2.

4.1 FDCM - MODULES 1-3

For the implementation of CSM we use the semi-submersible as an offshore platform and the technical details of semi-submersible used herein are listed in Table 1(A). The 'Ansys Design Modeler (ADM)' of Ansys AQWA**TM is used for the geometric modeling of semi-submersible. The surface body of semi-submersible is discretized into two sets: Sets of diffracting and non-diffracting elements. In the process of discretization as diffracting/non-diffracting bodies as panels with singularities, there are always restrictions imposed on the total number of elements to ensure reasonable accuracy and computational efficiency.

In the Ansys AQWA**TM the total number of elements are restricted to 18000 and out of these only 12000 at most can be grouped into the diffracting set. We name this 2/3 strategy and utilize this implying that it is preferred to ensure at least 2/3 of the total elements to diffracting set. E.g. if the total number of elements are 24000 then the diffracting set will be at least 16000. These - diffracting elements - are below the draft line and the non-diffracting elements are above the draft line and the resulting mesh allocating strategy is listed in Table 1(B).

4.2 FDCM - MODULES 4-5

The diffraction and radiation analyses are done in the 'Frequency Domain (FD)' and implemented

in the Ansys AWQA**TM to compute the free floating hydrostatic stability and RAOs for the offshore platform.

4.3 TDCM - MODULES 1-3

Once the computations of the FD are complete the TD computations start with an input from the FDCM. The technical details of marine riser used in the TDCM are listed in Table 1(C). The initial input for marine riser is the geometric and material details and after the basic hydrostatic analysis the discretization of marine riser is done.

In the existing literature the desired technical details of marine riser that are important in the analysis have not been reported in-detail and because of this the results are hard to reproduce. Furthermore, the marine riser parameters are governed by the specific applications aimed at the particular location and because these details are important from the practical design considerations there is lack of support and willingness from the offshore companies to disclose these details. Additionally, the length of marine riser is governed by many factors, e.g. the pre tension, angle of inclination of the marine riser from platform, differential location of the well head with respect to the offshore platform, current velocity, waves, and other environmental forces causing motions in the offshore platform and marine riser (i.e., a higher lay down length compensates larger motions), and geometric and material properties of the marine riser, etc. A list of the marine riser technical details available from the existing literature is reported in Table 1(C) and we can see that most of the details are missing. As mentioned in Table 1(C) various researchers have considered different current velocities, i.e., 0.06 m/s (Morooka and Tsukada (2013)) to 2 m/s (Ahmad and Datta (1989)). Also, in the high current regimes, e.g., Gulf of Mexico, the current velocities can reach up to 2 m/s and beyond during storm/surge, etc., for more details see Gordon (1967) and Sturges and Leben (2000).

Because of these reasons we considered current variations from 1.5 m/s to 2.25 m/s. Additionally, since the VIV is a current driven phenomenon, considering low current velocities does not serve the purpose of the analysis. An efficient design of the marine riser demands that the total length is kept as close to the operating water depths as possible. However, this is rarely achieved in the practice because the platform location is difficult to change once it is moored and the locations of wells being drilled are governed by the geological considerations. Based upon the analysis of present data we observe that the total length of marine riser varies from 1.4 to 3 and higher times the operating water length and the length of suspension varies from 1.2 to 1.6 times the operating water length. The length of suspension - length of riser from platform to touch down - is critically important in the dynamic analysis and the initial length of around 250 m is more so because on this length the current variation is maximum and all the ocean surface forces also act closer to this length.

In our work, we keep the length of suspension at 1.2 times of the operating water depth and we do not focus on the lay down length because we assume that the marine riser is connected from the offshore platform end to the well head with bare minimum requirement of the lay down length. Also, in our case the lay down length is more to ensure proper connection and less to compensate for motion. Based upon this the technical details of marine riser used in this work are listed in Table 1(D). Although, the steel density is conventionally around 7850 kg/m^3, a marine riser in the field is heavily stiffened, has buoyancy modules and lots of hanging weights to ensure a desired shape. All these essentially increase the density and from analysis point of view it is important to settle for an equivalent density that is approximately closer to the real field. Because of these reasons, we

consider the density of riser/steel as 8200 kg/m^3 and this approach is common with others, e.g., (Khan *et al.* 2011).

Herein, we consider the sea states from 4 to 9 and for these the information regarding wave heights and wave periods is reported in Table 1(D), for more details see Journee and Massie (2001). We consider the marine riser as a column subjected to lateral and in-line loads and the length of each element is important because it affects the computational efficiency and accuracy. Based upon the review of existing literature we propose a simple guideline: An elemental length of around 1.25 m for the sea states up to 9 and current velocity up to 2.25 m/s.

This initial length is implemented and checked against the total length that is being analysed and adjusted to ensure the total number of elements is integer and some adjustment is done to ensure that the top and bottom ends are properly connected to the offshore platform and touchdown. After these considerations we arrive at the elemental length of 1.39 m and the total number of elements is 863. This discretization strategy of the marine riser is listed in Table 1(E). After the discretization, each of the marine riser elements is modelled as a multi degree of freedom damped spring-mass system and these have been shown already in Figs. 5(A) and 5(B).

4.4 TDCM - MODULE 4

After modelling the marine riser with geometric and material details, the structural boundary conditions are implemented. The bottom end of the riser is assumed to be fixed on the sea bed and the top end of the marine riser is assumed to be rigidly connected to the offshore platform, i.e., the motions of offshore platform are transferred to the marine riser and no degree of freedom is released or restricted. The RAOs of the offshore platform computed in the FDCM are converted from their FD to motion time histories using transfer functions. These motion histories of the offshore platform and other loads (e.g., torsion, if applicable?) are transferred to the top end of marine riser in terms of the structural loads. These are integrated to the marine riser such that as the waves and current proceed at each of the time steps of simulation the motion and load histories are transferred from the offshore platform to marine riser and the coupled motion analysis is done.

4.5 TDCM - MODULE 5

Herein, the static analysis of integrated system (i.e., marine riser and offshore platform) is done to achieve the equilibrium position and as a result of the static analysis the natural frequencies and time periods of marine riser are computed. We observe from the results of static analysis that each of the even modes dominates only in the in-line and axial directions rather than in the transverse direction. Each of the odd modes dominates in the transverse direction as compared to the axial and in-line directions. These observations are in agreement with results from (Vandiver *et al.* 2006).

In general, within the existing literature only the lower modes are considered in the vibration analysis. However, in the case of marine riser neglecting the higher modes tend to under predict the fatigue damage of marine riser as the contribution of higher modes is expected to be significant especially at the higher current velocities, waves and other parameters. At present, we do not focus on the detailed modal analysis to compute their exact contributions and we only observe. We believe that a separate modal analysis is needed to understand the behavior of these higher modes in-detail.

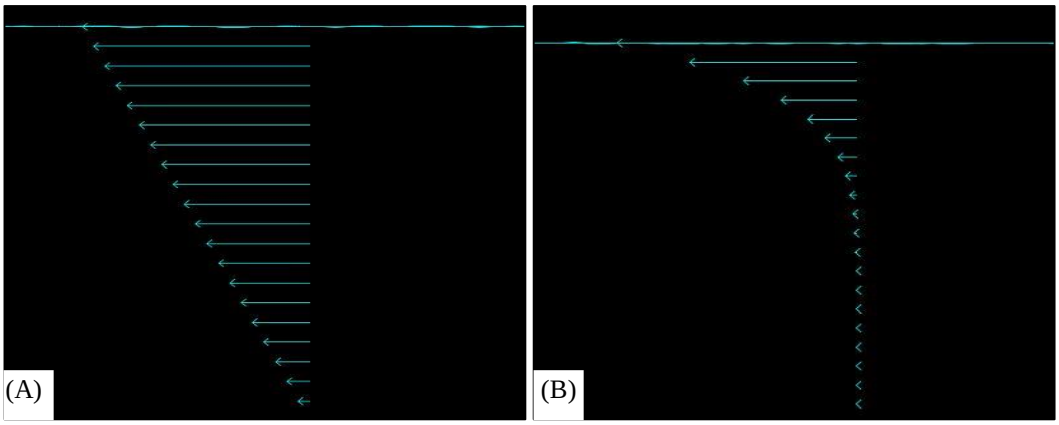

Fig. 8 (a) Linear current profile, and (b) Power law current profile

4.6 TDCM - MODULE 6-7

Herein, the dynamic simulation starts and the marine riser get subjected to ocean loads, i.e., wave, current, VIV and platform motion, etc.

Herein, only a particular sea state is assumed to occur for the entire duration of the analysis. Present thesis considers a total of 25 years of life of structure by using 1000 second simulation. This assumption is much more than the other standard time durations considered by different researchers, e.g., (Khan *et al.* 2011) and (Ulveseter *et al.* 2018) considered 100 seconds and Zhang and Qiu (2018) considered of 150 second of time in their analysis. Additionally, in terms of the design of offshore structures, the sea states of 4 to 6 are usually operating sea states and the sea states of 7 to 9 are considered as the survival sea states, e.g., for details see Coe and Neary (2014). Therefore, we have considered sea states of 4 to 9 in the present paper.

Marine riser fatigue damage analysis is reported under the actions of different ocean load combinations and these combinations are listed in Table 2. We study the effects of nature of current profile in-detail and accordingly compute the fatigue damage index, i.e., linear and power law variations.

At the end of dynamic simulation the responses and load time histories of the marine riser at various elements are known. However, since the number of load cases presented here is very large so instead of presenting the histories, we focus only on the presentation of results related to the computation of fatigue damage index. Figs. 8(a) and 8(b) show two different current profiles, i.e., linear and power law variations. These have been considered in the present work.

4.7 TDCM - MODULE 8-9

The results of dynamic simulations are imported for the post-processing of fatigue damage computations of marine riser. The first step in the computation of fatigue damage index is to compute the number of load cycles and this is done with the rain flow counting method. Then the stress cycles are computed and the cumulative fatigue damage index is computed by using the Miner's rule.

Table 1 (A) Technical details of semisubmersible adapted from Domala *et al.* (2014) and Gosain *et al.* (2017), (B) Details of the 2/3 mesh allocation strategy for the offshore platform, (C) List of the marine riser technical details available from the existing literature, (D) Technical details of marine riser used in this work, and (E) Discretization strategy of riser as finite element

(A)

Parameter	Value	Reference
Pontoon length	91.10 m	Ahmed and Datta (1989)
Pontoon breadth	11.92 m	Khan *et al.* (2011)
Pontoon height	6.22 m	Rivero-Angeles *et al.* (2013)
Column size (square section)	10.4 m X 10.4 m	Morooka and Tuskada (2013)
Height of column	35.23 m	Kunpeng *et al.* (2015)
Pontoon spacing	74.89 m	
CG from keel	23.80 m	
X meta centric height	04.20 m	
Y metacentric height	06.83 m	
X radius of gyration	34.90 m	
Y radius of gyration	34.10 m	
Z radius of gyration	39.40 m	
Draft	32.45 m	
Weights	24741 (tons)	

(C)

Operating water depth (in m)	Total length, length of riser from platform to touch down, lay down length	Current velocity, sea states	Wave spectrum
500 m	500 m, NK, NK	2 m/s, 9 (significant wave height 15 m)	NK
1800 m	2485 m, NK, NK	1.4 m/s, 7-8	PM spectrum
1800 m	2720 m, 2023 m, 697 m	NK, 1-5	PM spectrum
900 m	2066 m, 1300 m, 766 m	0.05 to 0.07 m/s, NK	NK
1000 m	1400 m, NK, NK	1 m/s, NK	NK

NK = Not known.

(B)

Total number of elements = Diffracting elements + Non-diffracting elements = 18000

S. No.	Analysis	Number of diffracting elements (2/3 of the total)	Number of non-diffracting elements (1/3 of the total)
1	Numerical analysis	12000	6000

(D)

Operating water depth (m)	1000
Riser length (m)	1200
Riser inner diameter (m)	0.407
Riser outer diameter (m)	0.429
Effective weight (kN/m)	1.1320
Top tension (kN)	3375.624
Water density (kg/m^3)	1025
Steel density (kg/m^3)	8200
Drag coefficient	1.0
Inertia coefficient	1.0
Surface current velocity (m/s)	1.5 to 2.25 m/s and the variations as per the load case
Modulus of elasticity (N/m^2)	2.07e11
VIV modeling	Wake oscillator model

(E)

S. No.	Analysis	Number of elements	Length of each element
1	Finite element analysis	863	1.39 m

Total length of marine riser = Number of elements * Length of each element

Wave load spectra - JONSWAP spectrum from Hasselmann *et al.* (1973)

Sea states 4 to 9 (wave height in m; and period in seconds) - 4 (1.88,8.80), 5(3.28,9.7), 6(5,12.4), 7(7.5,15.0), 8(11.5,16.4), 9(14,20)

5. Verification and validation of proposed computational model

Proposed CSM is implemented in industrially used standard soft solution systems (i.e., OrcaFlex*TM and Ansys AQWA**TM), Ms-Excel***TM, and C++ programming language using its object oriented features. The non-linear analysis of deep water marine riser is an important problem in the design and analysis of offshore structures. Any CSM needs to be verified and validated for its accuracy, applicability and efficiency through the comparison with either the experimental results or similar numerical results or both.

On the problem related to marine risers, the experimental studies are rare because they are prohibitively expensive and have strong industrial significance and hence reluctance to publish and make the results available in the public domain. As was mentioned previously, in Table 1(C), even most of the existing literature on numerical studies does not offer sufficient details that are essential for reproducing the results. In this environment of limited availability, to verify and validate the CSM, we use the results of (Khan *et al.* 2011). They studied the non-linear dynamic analysis of deep water marine riser in the FD and their computational model was implemented in the Abaqus FEA****TM software solution system.

5.1 Modeling difference between the two models

In (Khan *et al.* 2011) the computational modeling of the marine riser was done by using the tensioned beam elements but they did not report the end to end connectivity details, i.e., co-ordinates of the ends of marine riser. Because of this it is difficult to exactly match their structural boundary conditions and instead of the assumption as a tensioned beam we opt for the tensioned catenary.

It is important to note here that the basic governing differential equations for the marine riser are same in the cases of tensioned beam and tensioned catenary with only some minor variations in the curvature and low down length, i.e., curvature and low down length are higher for the catenary in comparison with tensioned beam.

5.2 Technical details of the marine riser

Technical details of marine riser are listed in Table 3 (A) and these are adapted from (Khan *et al.* 2011). They focused only on certain wave height, current velocity and zero crossing period and these ocean environmental parameters are mentioned in Table 3 (B).

5.3 Comparison of the results of static analysis

For the marine riser of Table 3(A) and under the conditions of Table 3(B), we compute the natural frequencies and compare them with results from (Khan *et al.* 2011). The discretization strategy of marine riser in the FEA is listed in Table 3(C). Table 3(D) shows the comparison of computed natural frequencies and we observe that the results show good agreement and the errors are marginal, i.e., maximum error = 23.8993 % (i.e., happening in the under prediction of results in the 4^{th} mode), and minimum error = 1.730317 % (i.e., happening in the over prediction of results in the 1^{st} mode).

Furthermore, we note that our CSM computes the natural frequencies higher to the (Khan *et al.* 2011) in the lower modes (i.e., 1, 2 and 3) and after that in the higher modes the trend is reversed.

Table 2 List of different ocean load combinations

Load case	Current velocity [m/s]	Current profile	Load case	Current velocity [m/s]	Current profile	Load case	Current velocity [m/s]	Current profile
4.1.01	1.5	Linear	5.1.01	1.5	Linear	6.1.01	1.5	Linear
4.1.02	1.5	Power law	5.1.02	1.5	Power law	6.1.02	1.5	Power law
4.2.01	1.75	Linear	5.2.01	1.75	Linear	6.2.01	1.75	Linear
4.2.02	1.75	Power law	5.2.02	1.75	Power law	6.2.02	1.75	Power law
4.3.01	2.0	Linear	5.3.01	2.0	Linear	6.3.01	2.0	Linear
4.3.02	2.0	Power law	5.3.02	2.0	Power law	6.3.02	2.0	Power law
4.4.01	2.25	Linear	5.4.01	2.25	Linear	6.4.01	2.25	Linear
4.4.02	2.25	Power law	5.4.02	2.25	Power law	6.4.02	2.25	Power law
Load case	Current velocity [m/s]	Current profile	Load case	Current velocity [m/s]	Current profile	Load case	Current velocity [m/s]	Current profile
7.1.01	1.5	Linear	8.1.01	1.5	Linear	9.1.01	1.5	Linear
7.1.02	1.5	Power law	8.1.02	1.5	Power law	9.1.02	1.5	Power law
7.2.01	1.75	Linear	8.2.01	1.75	Linear	9.2.01	1.75	Linear
7.2.02	1.75	Power law	8.2.02	1.75	Power law	9.2.02	1.75	Power law
7.3.01	2.0	Linear	8.3.01	2.0	Linear	9.3.01	2.0	Linear
7.3.02	2.0	Power law	8.3.02	2.0	Power law	9.3.02	2.0	Power law
7.4.01	2.25	Linear	8.4.01	2.25	Linear	9.4.01	2.25	Linear
7.4.02	2.25	Power law	8.4.02	2.25	Power law	9.4.02	2.25	Power law

Notation: In the load case definition the first number indicates the sea state (i.e., 4 means 4th sea state), second number indicates the current velocity (i.e., 1 means 1.5 m/s, 2 means 1.75 m/s, 3 means 2.0 m/s, and 4 means 2.25 m/s) and third number indicates current profile with the VIV (i.e., 01 means the linear current profile and 02 means the power law current profile)

In general, our computed results are closer to the results of (Khan *et al.* 2011) in odd modes in comparison to the even modes. We note that the errors are higher in even modes and this can be because of the medium current velocity considered by (Khan *et al.* 2011). In the low to medium current velocities the lower modes are more likely to be excited and in the higher current velocities the modes dominate the vibration. Also, the odd modes are in cross-flow direction and even modes are in the in-flow direction. Although, numerically, the differences are minor, the differences exist. The differences are because of multiple reasons, e.g., their length of element and number of elements are not known, no information about the end-to-end connectivity with boundary co-ordinates, differences in the tensioned beam and catenary conditions, and differences in the software solution systems. Fig. 9(A) shows the comparison of computed natural frequencies by our CSM and (Khan *et al.* 2011).

5.4 Comparison of the bending stresses

After comparing the results of static analysis, we next focus on comparing the results of dynamic analysis. We compute the bending stresses and compare them with (Khan *et al.* 2011). This is shown in Figs. 9(B) and 9(C) and the comparative results are listed in Table 3(E). We

Table 3 (A) Technical details of the marine riser adapted from (Khan *et al.* 2011), (B) Ocean environmental parameters adapted from (Khan *et al.* 2011), (C) Discretization strategy of marine riser in the FEA, (D) List of the comparison of computed natural frequencies by our CSM and (Khan *et al.* 2011), and (E) List of the comparison of computed bending stresses by our CSM and (Khan *et al.* 2011)

(A)

S. No.	Parameters	Value
1	Water depth (m)	1800
2	Riser length (m)	2485
3	Riser inner diameter (m)	0.407
4	Riser outer diameter (m)	0.429
5	Effective weight (kN/m)	1.1320
6	Top tension (kN)	3375.624
7	Water density (kg/m^3)	1025
8	Steel density (kg/m^3)	8200
9	Drag coefficient	1.0
10	Inertia coefficient	1.0
11	Surface current velocity (m/s)	1.4
12	Modulus of elasticity (N/m^2)	2.07e11
13	Wave load spectra	JONSWAP

(B)

S. No.	Parameters	Value
1	Significant wave height, sea state	9.5 m, 8
2	Zero crossing period	9.86 s
3	Current velocity	1.4 m/s

(C)

S. No.	Analysis	Number of elements	Length of each element
1	Finite element analysis	1787	1.39 m (rounded numerical value)

Total length of marine riser = Number of elements * Length of each element = 1787 * 1.39 = 2485 m.

(D)

Mode number	Computed natural frequency (in rad/s) by our CSM - (1)	Computed natural frequency (in rad/s) by Khan *et al.* (2011) - (2)	% Change = (((1)-(2))/(2))*100
1	0.0899296	0.0884	1.730317
2	0.1651012	0.1617	2.103401
3	0.1829364	0.1737	5.317444
4	0.1832504	0.2408	-23.8993
5	0.2783296	0.3092	-9.98396
6	0.2789576	0.3225	-13.5015
7	0.373032	0.4012	-7.02094
8	0.3779932	0.4485	-15.7206
9	0.4649712	0.4827	-3.67284
10	0.465348	0.5643	-17.5354
11	0.5541472	0.5776	-4.06039
12	0.5574756	0.6454	-13.6232
13	0.6440768	0.7084	-9.08007
14	0.6442024	0.728	-11.5107
15	0.737586	0.8108	-9.02985

(E)

Details	Computed bending stress by our CSM - (1)	Computed bending stress by Khan *et al.* (2011) - (2)	% Change = (((1)-(2))/(2))*100
Maximum	95.13 N/mm^2	70 N/mm^2	35.9
Minimum	0 N/mm^2	0 N/mm^2	0
Location	683.679 m	440 m	35.64

observe from the results that the trend of variation of bending stresses in both the cases is matching reasonably.

However, due to the differences in modeling techniques as mentioned before, the computed location of the maximum bending stresses (i.e., compressive and tensile bending stresses) are different.

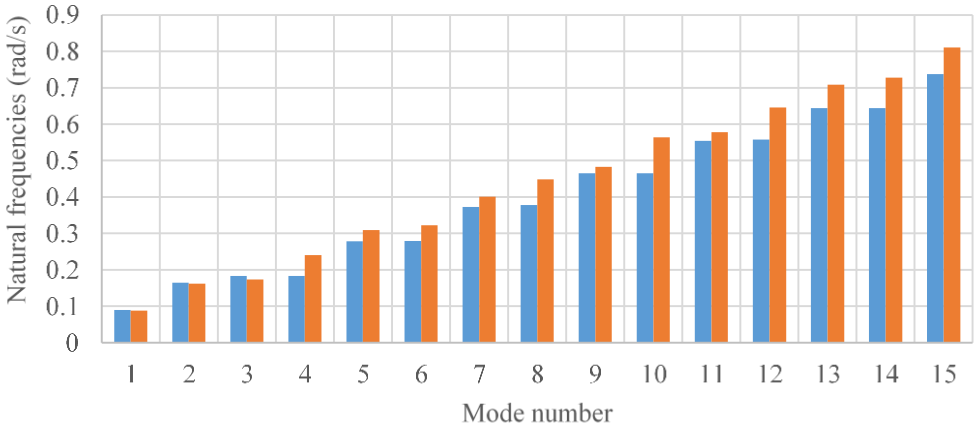

(A)

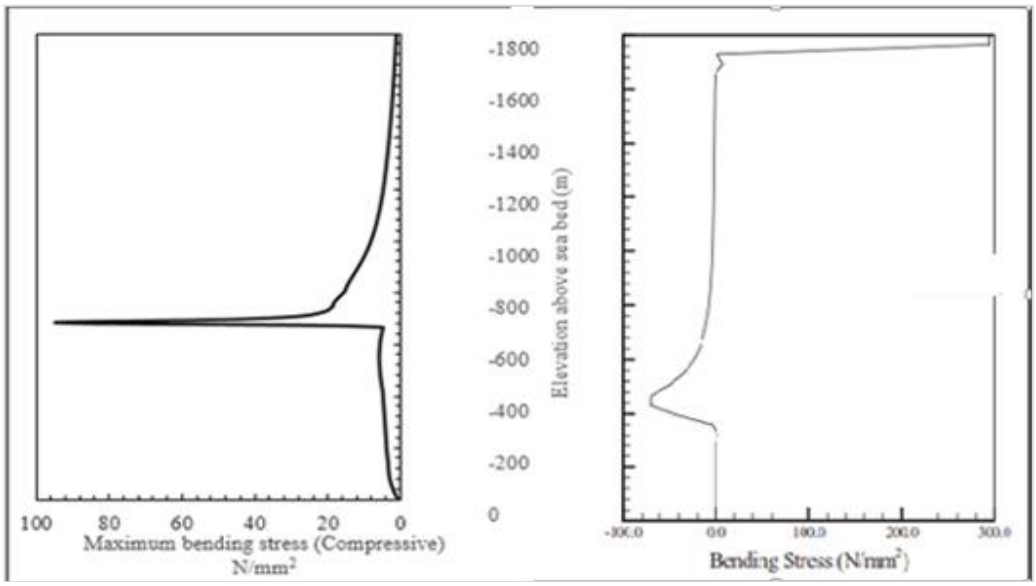

(B) (C)

Fig. 9 (A) Comparison of the computed natural frequencies by our CSM and (Khan *et al.* 2011), (B) Comparison of bending stress - Proposed CSM, and (C) Comparison of bending stress - (Khan *et al.* 2011)

In the marine riser analysis, the length from offshore platform to the touch down point is critically important because normally it is under compression and more susceptible to the buckling failure. The length from touch-down point to wellhead is expected to be in tension and though the tensile stresses will be higher but they are less likely to fail in tension.

Our computed results follow the conventional pattern as discussed before and we note that the computed maximum compressive bending stress is 95.13 N/mm^2 at - 683.68 m along the length of riser, i.e., being measured from the mean sea level and it is negative because of the convention followed by us as we consider depth positive in the upward direction and negative in the downward direction from mean sea level.

A comparison with (Khan *et al.* 2011) is shown in Figs. 9(B) and 9(C). We can observe from the comparison that the results show a match in trend. But, our results differ from the results of (Khan *et al.* 2011) in the determination of the location and maximum value of the bending stress. The differences are because of multiple reasons: Modeling differences, differences in the end conditions and connections, lack of information about the touch-down point and lay down length, and differences in the natural frequencies. Furthermore, because of the lack of information about the touch-down point and lay down length, the tensile stresses cannot be computed. A trial and error computation of the touch-down point is neither practical nor computationally feasible and an un-correct assumption of the touch-down point and lay down length will make the comparison meaningless. Hence, we focus only on the length that is equal to the water depth only, i.e., 1800 m.

From the presented results here in Section 5, cautiously we can conclude that the proposed CSM computes the results that are in fair agreement with the available results from the literature, (Khan *et al.* 2011), in terms of pattern and nature of variations. However, as we have mentioned before, the existing results are difficult to reproduce because in general there exists a lack of detailed information available in the existing literature on marine riser. Within the limited but encouraging comparison we believe that the proposed CSM can be taken forward for the further dynamic analyses. Now, using the CSM we report the results of an extensive dynamic analysis of deep water marine riser to investigate the fatigue damage analysis under different loading conditions.

6. Numerical example with suitable geometry of semisubmersible and riser

A primary idea in the proposed CSM is to compute the fatigue damage indices of deep water marine riser under different ocean environmental loads in the computing based simulation model with the overall integration of motion of the offshore platform and VIV forces, etc.

6.1 Detailed description of the marine riser

A 1200 m long steel catenary riser is considered for the analysis in 1000 m deep water subjected to various combinations of loads and we assume the location to be in the North Sea and accordingly, we consider the sea states, current velocities, and VIV loads etc. These have been mentioned earlier in Tables 1 and 2.

Our analysis has shown that the fatigue damage of marine riser is mainly current driven and it is because of the dominance of VIV in fatigue damage which is current driven. This agrees well with the established literature, e.g., (Gao *et al.* 2011). Because of this reason we focus on the regimes of high current velocities, i.e., 1.5 m/s, 1.75 m/s, 2.0 m/s and 2.25 m/s. We consider different sea states, 4 to 9, and they represent the variations from the operating sea states (i.e., 4/5/6) to the surviving sea states (i.e., 7/8/9).

A significant limitation in the existing literature is that most of the available research results have reported either the results on predominantly bare marine riser or they excite the marine riser

Table 4 Results of the static analysis

Mode no.	Period (s)	Mode type	Inline (%)	Transverse (%)	Axial (%)
1	79.13883	Transverse	0.2	99.8	0
2	64.21497	Inline dominating	86.8	0.2	13
3	38.15133	Transverse	0.2	99.8	0
4	34.12330	Inline dominating	90	0.2	9.8
5	25.21476	Transverse	0.2	99.8	0
6	22.48965	Inline dominating	88.3	0.2	11.5
7	18.85271	Transverse	0.2	99.8	0
8	17.1607	Inline dominating	90.7	0.2	9.2
9	15.06114	Transverse	0.2	99.8	0
10	13.74659	Inline dominating	89.9	0.2	9.9
11	12.54076	Transverse	0.2	99.8	0
12	11.56307	Inline dominating	91.2	0.2	8.7
13	10.74252	Transverse	0.2	99.8	0
14	9.93441	Inline dominating	90.8	0.2	9.1
15	9.39416	Transverse	0.2	99.8	0
16	8.74509	Inline dominating	91.6	0.2	8.2
17	8.34520	Transverse	0.2	99.8	0
18	7.78955	Inline dominating	91.4	0.1	8.4
19	7.50563	Transverse	0.2	99.8	0
20	7.03987	Inline dominating	92.1	0.1	7.8
21	6.81831	Transverse	0.2	99.8	0
22	6.41038	Inline dominating	92	0.1	7.8
23	6.24517	Transverse	0.2	99.8	0
24	5.89372	Inline dominating	92.5	0.1	7.3
25	5.7599	Transverse	0.2	99.8	0
26	5.44703	Inline dominating	92.5	0.1	7.3
27	5.3437	Transverse	0.2	99.8	0
28	5.06888	Inline dominating	93	0.1	6.9
29	4.98277	Transverse	0.1	99.8	0

parametrically without any input from the dynamics of offshore structure. We address this limitation in the present work and we integrate the dynamics of offshore structure with marine riser and consider all the six DOFs motion dynamics of offshore platform. This results into the coupled analysis.

Primarily, our focus is to compare the fatigue damage indices of marine riser with different conditions, i.e., fatigue damage comparison of riser with and without VIV, and fatigue damage comparison of riser under linear and power law current profiles with various combinations of loads, etc. These details have been reported earlier in Tables 1 and 2.

7. Results and discussion of numerical example

7.1 Static analysis

Using the details of Tables 1 and 2, the results of static analysis are reported in Table 4. We can

observe from the results that each of the even modes is dominating only in the in-line and axial directions rather than in the transverse direction. Also, each of the odd modes is dominating in the transverse direction as compared to the axial and in-line directions. Additionally, in the even number modes, the contribution of inline motion is significant along with fair contribution from the axial motion. This distribution remains more or less the same even at the higher even number of modes. On the other hand all the odd number modes are dominated by the transverse motions and other contributions are non-significant (i.e., close to 0). In our opinion this implies that the odd number of modes will be easier to address for fatigue damage control in comparison to the even number of modes because stiffening will be in 2 dimensions for the even number and in 1 dimension for the odd number of modes.

A moving bluff body in fluid experiences two forces: lift and drag. In the case of offshore structures the used shapes are normally bluff body (i.e., cylindrical structures) and they are positioned at certain location or moved/towed at very low speed. In the field conditions - operational and survival - an offshore structure does not experience significant drag force but lift force. This generated lift is in the perpendicular direction to the incoming flow and this is dominating across the wide range of incoming flow velocities. This lift acts as the excitation force in first mode of vibration and being the lift it will in the transverse direction. A lift in the transverse direction creates an oscillating flow. Because of the fluid's viscosity, the flow around the bluff body slows down while in contact with its surface and this form the boundary layer.

A change in the velocities will result into changes in the pressure because of the Bernoulli's equation. Later, at some point, the boundary layer will separate from the body because of its excessive changes resulting into sharp curvature. Then, the vortices are formed and they change the pressure distribution along the surface.

Furthermore, if the vortices are not formed symmetrically around the body (i.e., with respect to its centre line plane), then the lift forces developed on each side of the body, will be different. This difference leads to a motion that is transverse to the incoming flow.

This differential motion changes the nature of the vortex formation and lead to limited motion amplitudes. And, in this differential motion the vortex shedding happens from the marine riser surface and that causes the inline and axial motions. Additionally, we note here that in general as per the best of our knowledge most of the existing literature does not analyze the contribution of an individual motion (i.e., inline, axial and transverse motions). This is a limitation because ignoring an individual motion is likely to result into the under prediction of fatigue damage. Also, the contribution of an individual motion will determine the positioning of stiffeners to reduce the fatigue damage accordingly, i.e., axial, inline and transverse stiffeners.

Herein, we consider only few selected modes for the vibration analysis as per the available conventions in the literature, i.e., (Lei *et al.* 2014) considered 29 modes and (Khan *et al.* 2011) considered 15 modes. Although, from the practical considerations it is not feasible to analyze the structure in higher modes of the vibration as it is less likely to vibrate in these modes, still it is analyzed because of the following reasons:

- A marine riser along with the platform is expected to work in severe harsh ocean environment and it is subjected to the loads and motions because of the VIV and VIM, etc. Some of these loads are of high magnitude and high/low frequency, with low magnitude and high frequency, and low magnitude and low frequency.

A load with high magnitude and high frequency and/or low magnitude and high frequency will excite the higher modes of vibration. And, although the chances of that occurrence may be low, if it happen it is likely to cause significantly high fatigue damage. Because of this reason, most of

existing literature has advocated the importance of studying the higher modes up to 29, e.g., (Lei *et al.* 2014).

However, neglecting the higher modes tend to under predict the fatigue damage of marine riser as the contribution of higher modes is significant. We believe that a separate modal analysis is needed to understand the behavior of these higher modes. We note that the higher modes do not contribute in the axial direction and their contributions reduce as the mode increases.

7.2 Dynamic analysis

Dynamic analysis starts at the end of static analysis after obtaining the static equilibrium positions and eliminating the balance forces completely. In the dynamic analysis we consider different loads, i.e., wave, wind, current, VIV and platform motion, etc. Under the actions of various combinations (in reference to Table 2) of these loads, the dynamic analysis of marine riser is done to understand the qualitative and quantitative behaviors of the marine riser fatigue under various combinations of the loads.

As far as the dynamic analysis and the subsequent prediction of fatigue damage are concerned, there exist some important limitations in the existing literature, e.g.:

- Only the lower mode vibrations (i.e., first and second) are studied while ignoring the higher modes.

- Only the bare marine riser is considered while ignoring the coupled motion analysis because of the presence of offshore platform. And, even when the offshore platform's motion is considered it is considered as a single DOF input.

- Only a specific type of the current profile is considered while ignoring the others.

Herein, we address these above mentioned limitations and we focus on the fatigue damage analysis of deep-water marine riser under two case studies: Comparison of the fatigue damage with and without the VIV in the presence of coupled offshore platform motion analysis, and Comparison of the fatigue damage with two different current profiles (i.e. linear and power laws).

7.2.1 Current with linear variation

We consider the following cases:-

- Load cases 1.1 and 1.01 under different sea states and at the current velocity of 1.5 m/s with linear law: We report the results of without VIV and with VIV under different sea states at the current velocity of 1.5 m/s and assume linear law variation of the current. The idea here is to analyze the effects of VIV along with the sea states to arrive at some preliminary design guidelines that can be applied in the design process of marine riser.

Computed FDIs are shown in Figs. 10(A) and 10(B) for different sea states (4 to 9) at the current velocity of 1.5 m/s without the VIV and with the VIV, respectively. We note from the results that the computed FDI increases as the sea state increases in both the cases of without the VIV and with the VIV. As the higher sea states are characterized by the higher wave heights the structure is subjected to higher wave forces and a larger portion of the length of marine riser undergoes periodic/oscillatory forces (i.e. wave forces) at the higher sea states. This results into the larger FDI around the length that is close to the offshore platform. Presented results follow this and additionally we note the following:

- From Fig. 10(A), the computed FDI increases with the increase in sea states. This is obvious and the maximum computed FDI is occurring around the L^* = 1.0. That implies that around the TDP the maximum fatigue damage is likely to happen. In the presented results of Fig. 10(A) we

observe multiple peaks of the computed FDI, i.e., one peak is close to the top end connection of the offshore platform and marine riser and the second peak is close to the TDP. In the lower sea states (i.e., 4 to 7) the first peak is higher than the second peak and in the higher sea states (i.e., 8 to 9) the second peak starts dominating as mentioned in Table 5(A).

This is interesting because it implies that the motions induced by the offshore platform are significant and dominating in comparison to the motions of marine riser in the lower sea states. In the higher sea states the motions of the offshore platform becomes so high that they cause the marine riser to be lifted up and thereby cause the shift of TDP. Once the higher length of the marine riser is lifted up it increases its own motions and that results into the higher FDI in marine riser around the TDP. Our results reinforce the above mentioned discussion.

- From Fig. 10(B), the influence of VIV on fatigue becomes clear and we note that because the also VIV induces forces that are periodic/oscillatory and they can get coupled with the other forces (e.g., wave forces). This coupling of forces can imply the higher or lower motion amplitudes through the process of superimposition, e.g., even in a low state the forces and motions can get coupled, added and because of this addition a low sea state can also result into the high computed FDI.

Also, we note that the VIV is a phenomenon that is concentrated closer to the mean sea level (i.e., sea surface) and this coupled with wave forces implies that the length closer to the sea surface will be subjected to the high fatigue.

Presented results reinforce the above mentioned discussion. At the sea state of 4 we observe a higher computed FDI in comparison to 5 and 6 and there exist multiple peaks in each load case as mentioned in Table 5(A). This is because of the coupling as mentioned before.

Coupling effects are dominated by the amplitudes and phase differences and these will change in the sea states and modes of the vibration. Once they change the effects of superposition will not lead to addition or deletion of the motion amplitudes. This is clear after the sea state of 4 as the computed maximum FDI increases with the increase in sea states from 5 to 9.

- We consider two variations in the current profiles: Linear and power laws. The results of Figs. 10(A)-10(H) are for the variation with linear law. We note that in the linear law the rate of change of current velocity w.r.t. the depth is low and in the power law this rate is very high, i.e., implying that the current velocity will reduce sharply over the depth in power law variation, a current velocity of 1.5 m/s will reduce to 0.1 m/s at a depth of 600 m and 930 m in the cases of power and linear laws respectively.

This means that in the linear law variation a larger length of the marine riser will be subjected to higher current velocities than with the power law. And, that will result into the higher computed FDI closer to the connection of marine riser and offshore platform. Although, the VIV is a current driven phenomenon, the current velocity decreases sharply from the mean sea level to the ocean bed in the case of power law and a lesser length of the marine riser is subjected to the high current velocity. Because of this, the maximum computed FDI in the power law variation happens around the TDP rather than around the connection of marine riser and offshore platform as happens in the linear law variation. These results are analyzed in detail in Figs. 10 (I)-10(L) and 11(A)-11(D).

- Load cases 2.1 and 2.01 under different sea states and at the current velocity of 1.75 m/s with linear law: As previously, herein we consider the current velocity of 1.75 m/s and assume linear law variation of the current. The computed FDIs are shown in Figs. 10(C) and 10(D) for different sea states (4 to 9) at the current velocity of 1.75 m/s without the VIV and with the VIV, respectively. We note the following:

- Without the VIV the computed maximum FDI increases with an increase in the sea state and this trend is valid up to the sea state of 7 as mentioned in the Fig. 10(C). However, in the sea states

of 8 and 9, the computed maximum FDI is higher in the 8 in comparison to the 9. As before, herein we observe two peaks in each of the load cases, i.e., one is near to the connection between the offshore platform and marine riser and the second is near to the TDP as listed in Table 5(B). We further observe that in the higher sea state (i.e., 9) the second peak (i.e., near TDP) dominates and it has the maximum computed FDI. In the higher sea states it implies that the motions of the offshore platform become so high that they cause the marine riser to be lifted up and thereby cause the shift of TDP. As has been mentioned before, once the higher length of marine riser is lifted up it increases its own motions and that results into the higher maximum computed FDI in marine riser around the TDP.

- With the VIV, the computed maximum FDI increases with an increase in the sea states, except at the sea state of 4. The maximum computed FDI is higher in the sea state of 4 as compared to that in the sea states of 5 and 6. As has been mentioned before, the VIV generates motions that are periodic/oscillatory and depending upon the matching of amplitudes and phase differences between different motion wave, there can be a coupling of motions because of the waves and VIV. Once this happen, this will result into the computed higher FDI. We note that in the sea state of 4 there is strong coupling as compared to that in the sea states of 5 and 6 as shown in Fig. 10(D) and listed in Table 5(B).

As before, herein we observe two peaks in each of the load cases and they occur at the similar locations, i.e., near to the connection between offshore platform and the marine riser and near to the TDP. Furthermore, we observe from Table 5 (B) that in all the sea states the first peak (i.e., near to the connection between offshore platform and the marine riser) dominates and it has the maximum computed FDI.

The VIV is a current driven phenomenon and the current velocity decreases sharply from the mean sea level to the ocean bed. This decrease is different in both the linear and power laws. Although, the power law is closer to the realistic distribution of current, the linear law offers a very conservative estimation (i.e., on the much higher side than the power law) of the current profile across the depth. This conservative estimation can result into non-realistic computation of the FDI. In the real ocean/sea, in fact, after around 100 to 150 m it becomes constant and practically non-significant. Because of this reason, with the high current velocity and VIV, a length close to the mean sea level is subjected to very high forces and motions in comparison to the length that is downward of 150 m up to the TDP. Also, the motions because of the coupling of the VIV forces with other ocean loads (e.g., wave and current) can get magnified through superposition and this causes a higher susceptibility at the higher sea states and current velocities. And, at the high sea state and current velocity a significantly large length is subjected to very high FDI, i.e., for more details see Fig. 10(D), load case 9.2.01. We note that the second peak is occurring at the TDP because of the continuous compression and tension loads due to offshore platform motion acting on the marine riser.

- *Load cases 3.1 and 3.01 under different sea states and at the current velocity of 2.0 m/s with linear law:* Next, we consider the current velocity of 2.0 m/s and assume linear law variation of the current. The computed FDIs are shown in Figs. 10 (E)- and (10F) for different sea states (4 to 9) at the current velocity of 2.0 m/s without the VIV and with the VIV, respectively. We note the following:

- Without the VIV the computed maximum FDI increases with an increase in the sea state and this trend is valid up to the sea state of 7 as mentioned in the Fig. 10(E). However, in the sea states of 8 and 9, the computed maximum FDI is higher in 8 as compared to 9. Previous explanation reported for Fig. 10(C) is also valid here. Similar to Fig. 10(C), here also we observe two peaks in each of the load cases and they behave similarly to the case of current velocity of 1.75 m/s. The same previous explanation reported for Fig. 10(C) is also valid here.

- With the VIV, the computed maximum FDI increases with an increase in all the sea states. It implies that at the higher value of the current velocity the maximum computed FDI becomes proportional to the sea state in the presence of VIV. Similar to Fig. 10(C), here (Table 5(C)) also we observe two peaks in each of the load cases and they behave similarly to the case of current velocity of 1.75 m/s. The same previous explanation reported for Fig. 10(C) is also valid here.

- Load cases 4.1 and 4.01 under different sea states and at the current velocity of 2.25 m/s with linear law: Next, we consider the current velocity of 2.25 m/s and assume linear law variation of the current. The computed FDIs are shown in Figs. 10(G) and 10(H) for different sea states (4 to 9) at the current velocity of 2.25 m/s without the VIV and with the VIV, respectively. We note the following:

- Without the VIV the computed maximum FDI increases with an increase in all the sea states as mentioned in the Fig. 10(G) and listed in Table 5(D), it implies that at higher value of the current velocity maximum computed FDI becomes proportional to the sea state even in the absence of VIV. Similar to Fig. 10(C), here also we observe two peaks in each of the load cases and they behave similarly to the case of current velocity of 1.75 m/s. The same previous explanation reported for Fig. 10(C) is also valid here. In this load case, we observed that the first peak is dominating in the maximum computed FDI as listed in Table 5(D).

- With the VIV, the computed maximum FDI increases with an increase in all the sea states as shown in Fig. 10(H). It implies that at the higher value of the current velocity the maximum computed FDI becomes proportional to the sea state in the presence of VIV. Similar to Fig. 10(C), here also we observe two peaks in each of the load cases and they behave similarly to the case of current velocity of 1.75 m/s. The same previous explanation reported for Fig. 10(C) is also valid here. Computed maximum FDI and the location of the both peaks are listed in Table 5 (D).

7.2.2 Current with power law variation

We consider the following cases:

- FDI computation under the power law current variation without VIV for all load cases: Herein, we present the results of computed FDI of the marine riser for the current velocity of 1.5 m/s, 1.75 m/s, 2.0 m/s and 2.25 m/s for the various sea states (i.e., 4-9) under the action of power law current variation without VIV. The results of the computed FDI are presented in Fig. 7.5 and we noted the following.

- We note from the results of the Figs. 10(I)-10(L) that, computed FDI increases gradually from the sea state of 4 to 7, however in the sea state of 8 and 9, maximum computed FDI in the sea state 8 is slightly more than that in the sea state 9 and this is observed in the all the current velocity variations of 1.5 m/s, 1.75m/s, 2.0 m/s and 2.25 m/s. Also, we have observed that as the current velocity increases maximum computed FDI decreases for the corresponding sea states as can be seen from the Tables 6(A)-6(D). The reason of the above might be like power law current velocity produces higher damping motion of the marine riser at higher velocity.

- Another critical observation can be made from the results of Figs. 10(I)-10(L) and Tables 6(A)-6(D) is that here also we observed two peaks as we have observed in the case of linear current velocity and the happens to be at similar location i.e., one at near the connection point of the riser platform and the second is near the TDP zone. We can see that in almost all the load case second peak is dominating except few load cases like 8.1.2, 9.1.2, 8.2.2 and 8.3.2. However the changes in the computed maximum FDI are minor at those load cases.

Table 5 Magnitudes and locations of the computed FDI peaks for different load combinations and linear currents

Load case (without VIV)	Computed FDI (peaks)		Location (peaks)		Load case (with VIV)	Computed FDI (peaks)		Location (peaks)	
	Peak 1	Peak 2	Peak 1	Peak 2		Peak 1	Peak 2	Peak 1	Peak 2
(A) Linear current variation - 1.5 m/s current velocity.									
4.1.1	0.0511	0.0013	2.238	1020.1	4.1.01	0.8314	0.003	2.238	1018.6
5.1.1	0.2936	0.1000	2.238	1018.6	5.1.01	0.6571	0.0165	2.238	1109.7
6.1.1	0.4257	0.0295	2.238	1011.2	6.1.01	0.7842	0.0290	2.238	1012.6
7.1.1	0.8593	0.5001	2.238	1006.7	7.1.01	1.2328	0.5321	2.238	1005.2
8.1.1	3.348	3.430	8.20	1005.2	8.1.01	3.8340	2.1732	3.731	1003.3
9.1.1	2.536	2.830	2.230	1005.2	9.1.01	5.777	1.8239	3.731	1005.2
(B) Linear current variation - 1.75 m/s current velocity.									
4.2.1	0.0435	0.0010	2.23	1032.1	4.2.01	6.855	---	2.23	---
5.2.1	0.244	0.0080	2.23	1023.1	5.2.01	0.973	0.0098	2.23	1024.62
6.2.1	0.366	0.0231	2.23	1021.6	6.2.01	1.8153	0.025	2.23	1024.62
7.2.1	0.833	0.3701	2.23	1017.2	7.2.01	7.4598	0.382	2.23	1021.64
8.2.1	3.19	1.5443	2.23	1008.2	8.2.01	8.634	0.729	3.73	1026.11
9.2.1	2.541	2.91	7.46	1014.1	9.2.01	8.34	1.3092	2.23	1023.13
(C) Linear current variation - 2 m/s current velocity.									
4.3.1	0.0396	0.0007	2.238	1047.0	4.3.01	0.229	0.0013	2.238	1051.5
5.3.1	0.199	0.0046	2.238	1039.5	5.3.01	0.452	0.0057	2.238	1051.5
6.3.1	0.329	0.0156	2.238	1038.0	6.3.01	0.930	0.0197	2.238	1042.6
7.3.1	0.861	0.3181	2.238	1032.0	7.3.01	2.013	0.3058	2.238	1035.1
8.3.1	5.617	2.340	2.238	1024.6	8.3.01	5.40	0.8211	2.238	1041.4
9.3.1	3.231	2.218	2.238	1035.0	9.3.01	9.67	1.394	2.238	1042.5
(D) Linear current variation - 2.25 m/s current velocity.									
4.4.1	0.039	0.0007	2.238	1069.4	4.4.01	0.1104	0.002	2.238	1073.8
5.4.1	0.190	0.0039	2.238	1067.9	5.4.01	0.5267	0.009	2.238	1072.3
6.4.1	0.321	0.0124	2.238	1063.4	6.4.01	0.613	0.0241	2.238	1067.9
7.4.1	0.888	0.3150	2.238	1045.5	7.4.01	1.453	0.3056	2.238	1057.4
8.4.1	3.685	1.930	2.238	1045.5	8.4.01	11.0398	1.216	2.238	1061.9
9.4.1	5.111	3.736	2.238	1041.0	9.4.01	16.732	2.60	2.238	1054.5

7.2.3 Maximum computed FDI for the current variation power law with VIV

We consider the following cases:

- Load case 1.02 under different sea states and at the current velocity of 1.5 m/s with power law: Herein, we study the variation of current velocity with power law and report the results of comparison of the maximum computed FDI under the different current profiles: linear and power laws (i.e., 1/7) under different sea states. At the first we consider the current velocity of 1.5 m/s. The idea here is to analyze the effects of different current profiles on the FDI along with the different sea states (i.e., 4 to 9) to arrive at some preliminary design guidelines that can be applied in the design process of marine riser. It is known from the literature survey that the current profile

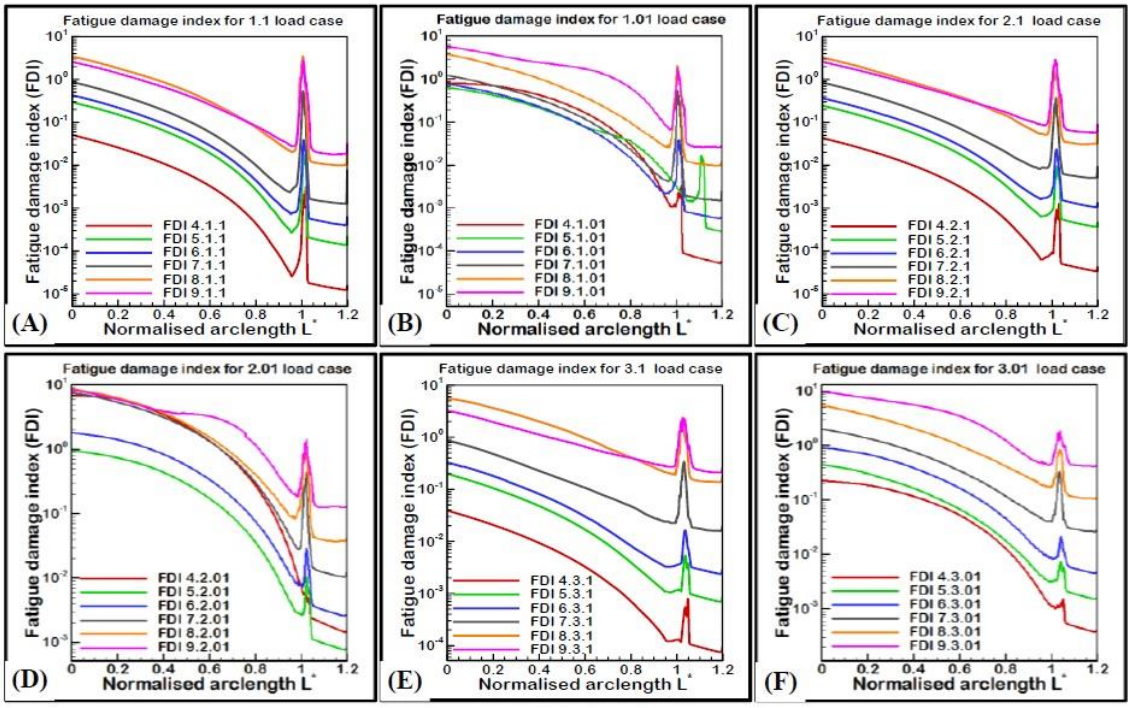

Fig. 10 Computed FDI and their comparisons under different sea states and load cases - Part 1

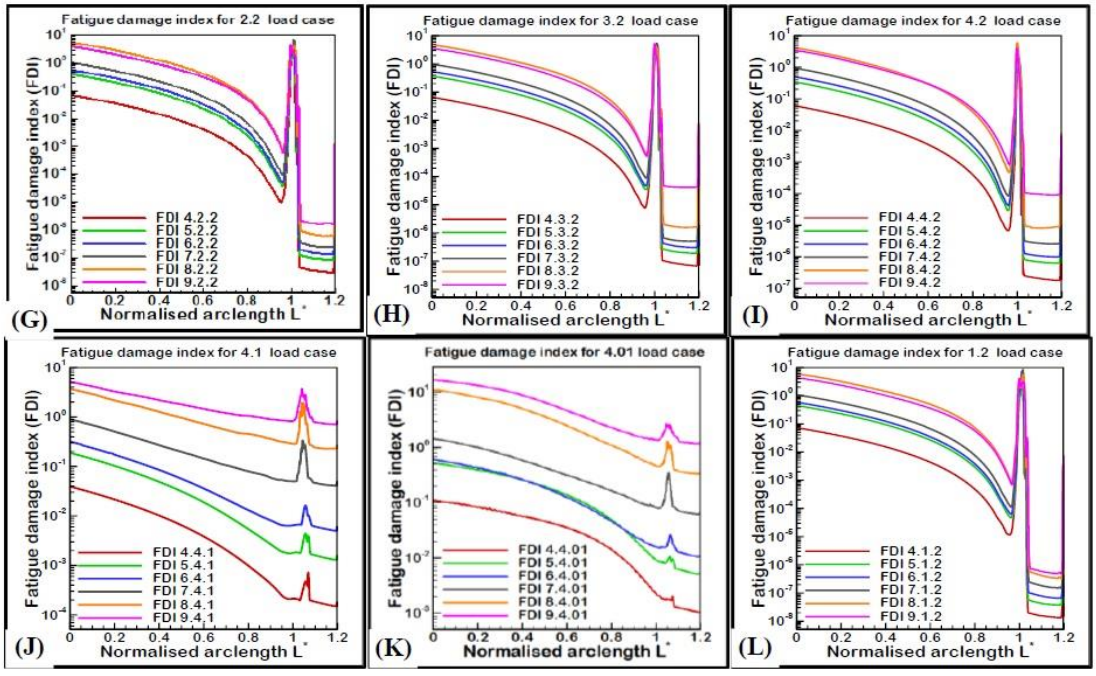

Fig. 10 Computed FDI and their comparisons under different sea states and load cases - Part 2

has a strong influence on the FDI of the marine riser and this is our motivation, i.e., for more details see (Gao *et al.* 2011). Previously, in Fig. 10 (Parts A and B) we have already presented the results of maximum computed FDI for 1.5 m/s current velocity under linear current variation. Now, we compute the FDI with the same loads as before but with power law variation and the results are shown in Figs. 11(A)-11(D). And from them we observe the following:

- The maximum computed FDI is higher under the action of power law current velocity as compared to that in linear current variation and this variation is valid till the sea state of 8. However, later under sea state of 9 the maximum computed FDI is higher under linear current profile as compared to that in power law current profile.

- The results of Fig. 11(A) are interesting and deeply meaningful for the design because they show that the FDI behavior under the combined effects of wave, current and VIV is highly complex, non-linear and defies simple explanations regarding monotonic increase or decrease.

- Essentially, the combined effects of wave, current and VIV are governed by the laws of superposition through interferences of the motions arising because of wave, current and VIV. As the wave and VIV both generate the periodic/oscillatory motions, they can cause significant reversal of stresses and that will cause the higher FDI. The current does not produce a periodic/oscillatory motion but it is one of the dominating parameters that contribute to VIV and the VIV generate periodic/oscillatory motions.

- A low to medium sea state (i.e., 4, 5, 6, and 7) is characterized by low to medium wave height and that will cause low amplitude motions.

The current variation under the power law will also result into the computation of lower current velocities and a low current velocity will restrict the VIV motions to the lower amplitudes only.

Now, these motions wave of low amplitudes - from wave, current and VIV - can get superimposed through the interference and can get added up depending upon the phase differences. Once they are added the amplitude will increase significantly and they being the periodic/oscillatory motions, there will be reversal of forces/stresses. This seems to be happening in the results of Fig. 11(A) at the low to medium sea state (i.e., 4, 5, 6, and 7).

- A high sea state (i.e., 8 and 9) is characterized by high wave height and that will cause high amplitude motions. The current variation under the linear law will also result into the computation of higher current velocities and a high current velocity will push the VIV motions to the higher amplitudes only. Now, these motions wave of high amplitudes - from wave, current and VIV - can get superimposed through the interference and can get added/cancelled up depending upon the phase differences. Once they are cancelled the amplitude will decrease significantly and they being the periodic/oscillatory motions, there will be reversal of forces/stresses. This seems to be happening in the results of Fig. 11(A) at the high sea state (i.e., 8 and 9) and it results into the computation of lower FDI in sea states of 8 and 9, and in 9 it is lower than 8. Also, because of the cancellation the differences in the computed FDI with the linear and power laws get reduced as the sea state increases.

- Table 7(A) lists the magnitude and location of the maximum computer FDI for 1.5 m/s current velocity with power law variation. As before, herein we observe two peaks in each of the load cases, i.e., one is near to the connection between the offshore platform and marine riser and the second is near to the TDP.

- We further observe that in all the sea states (i.e., 4-9) the second peak (i.e., near TDP) dominates and it has the maximum computed FDI. This implies that the current is less dominating because of the lower computed values with power law and the motions of the offshore platform along with VIV are dominating. These can cause the marine riser to be lifted up and thereby cause

Table 6 Magnitudes and locations of the computed FDI peaks for different load combinations and power law currents

Load case (without VIV)	Computed FDI (peaks)		Location (peaks)	
	Peak 1	Peak 2	Peak 1	Peak 2
(A) Power law current variation - 1.5 m/s current velocity without VIV.				
4.1.2	0.073	6.781	2.24	1012.0
5.1.2	0.455	6.403	2.25	1012.0
6.1.2	0.574	7.236	2.22	1014.79
7.1.2	1.055	8.405	2.24	1015.56
8.1.2	5.922	5.290	5.22	1015.56
9.1.2	4.280	4.090	5.25	999.25
(B) Power law current variation - for 1.75 m/s current velocity without VIV.				
4.2.2	0.069	5.193	2.240	1011.2
5.2.2	0.391	5.270	2.240	1012.6
6.2.2	0.551	6.257	2.240	1012.6
7.2.2	0.993	7.182	2.240	1014.8
8.2.2	5.349	4.228	5.220	1015.6
9.2.2	3.757	4.435	3.731	999.28
(C) Power law current variation - 2.0 m/s current velocity without VIV.				
4.3.2	0.065	4.210	2.240	1009.7
5.3.2	0.371	4.461	2.240	1009.7
6.3.2	0.530	5.352	2.240	1009.7
7.3.2	0.965	4.865	2.240	1012.6
8.3.2	4.785	4.506	5.220	1002.4
9.3.2	3.483	5.226	3.737	999.25
(D) Power law current variation - 2.25 m/s current velocity without VIV.				
4.4.2	0.620	0.913	2.300	1003.70
5.4.2	0.346	1.992	2.280	1000.70
6.4.2	0.501	2.949	2.280	1002.23
7.4.2	0.930	4.433	2.280	999.25
8.4.2	4.145	5.929	5.220	999.25
9.4.2	3.420	4.025	3.731	999.25

the shift of TDP. As has been mentioned before, once the higher length of marine riser is lifted up it increases its own motions and that results into the higher maximum computed FDI in marine riser around the TDP.

- Load case 2.02 under different sea states and at the current velocity of 1.75 m/s with power law: Previously, in Fig. 10(D) we have already presented the results of maximum computed FDI for 1.75 m/s current velocity under linear current variation. Now, we compute the FDI with the same loads as before but with power law variation and the results are shown in Fig. 11(B) and from them we observe the following:

- As with the case of 1.5 m/s with power law variation, the maximum computed FDI is higher under the action of power law current velocity as compared to that in linear current variation and

this variation is valid for the sea state of 5 and 6. However, later undersea states of 4, 7, 8 and 9 the maximum computed FDI is higher under linear current profile than that in power law current profile.

- We note from the results of Fig. 11(B) that the computed first peak of the FDI is increasing with an increase in the sea state. This is because of various reasons: first peak is close to the connection of marine riser and offshore platform and this area comes under the influence of current variation which is restricted to only a small portion in the power law variation, higher sea states cause higher amplitude motions in the offshore platform and the same are transmitted to the marine riser, and combined effects of the wave and current.

- Computed second peak of the FDI is more stable and does not show much variation with an increase in the sea state from 4 to 7. These results show the combined effects of wave, current and VIV and that are highly complex, non-linear and defies simple explanations regarding monotonic increase or decrease.

As mentioned previously, the combined effects of wave, current and VIV are governed by the laws of superposition through interferences of the motions arising because of wave, current and VIV. And, in the process of superposition the periodic/oscillatory motions, can get added up/cancelled up and they can cause significant reversal of stresses. These reversals cause the higher FDI. In the sea states - 4, 5, 6, and 7 - the low to medium amplitude motions along with the VIV motions of the lower to medium amplitudes get superimposed through the interference. In the process of interference and superposition they can get added/cancelled up depending upon the phase differences. This seems to be happening in the results of Fig. 10(J) at the sea state (i.e., 4, 5, 6, and 7).

- As has been mentioned previously, although a high sea state (i.e., 8 and 9) is characterized by high wave height and that will cause high amplitude motions. But, in the process of interference and superposition different motion waves can also get cancelled up depending upon the phase differences. This cancellation will reduce the reversal of stresses and bring down the FDI. This seems to be happening in the results of Fig. 11(B) at the sea state (i.e., 8, and 9).

- Table 7(B) lists the magnitude and location of the maximum computer FDI for 1.75 m/s current velocity with power law variation. As before, herein we observe two peaks in each of the load cases, i.e. one is near to the connection between the offshore platform and marine riser and the second is near to the TDP. We further observe that in all the sea states (i.e., 4-7) the second peak (i.e., near TDP) dominates and it has the maximum computed FDI. This implies that the current is less dominating because of the lower computed values with power law and the motions of the offshore platform along with VIV are dominating.

- Also, we further observe that in the sea states (i.e., 8-9) the first peak (i.e., near TDP) dominates and it has the maximum computed FDI. This is because of the higher motions of the offshore platform in higher sea states and less influence of current to the TDP with the power law variation. Herein, we do not observe that the marine riser is being lifted up and thereby causing the shift of TDP. As has been mentioned before, if no or only a small length of marine riser is lifted up it will not increase its own motions and that will result into the lower computed FDI in marine riser around the TDP.

- Load case 3.02 under different sea states and at the current velocity of 2.0 m/s with power law: Previously, in Fig. 10(F) we have already presented the results of maximum computed FDI for 2.0 m/s current velocity under linear current variation. Now, we compute the FDI with the same loads as before but with power law variation and the results are shown in Fig. 11(C) and from them we observe the following:

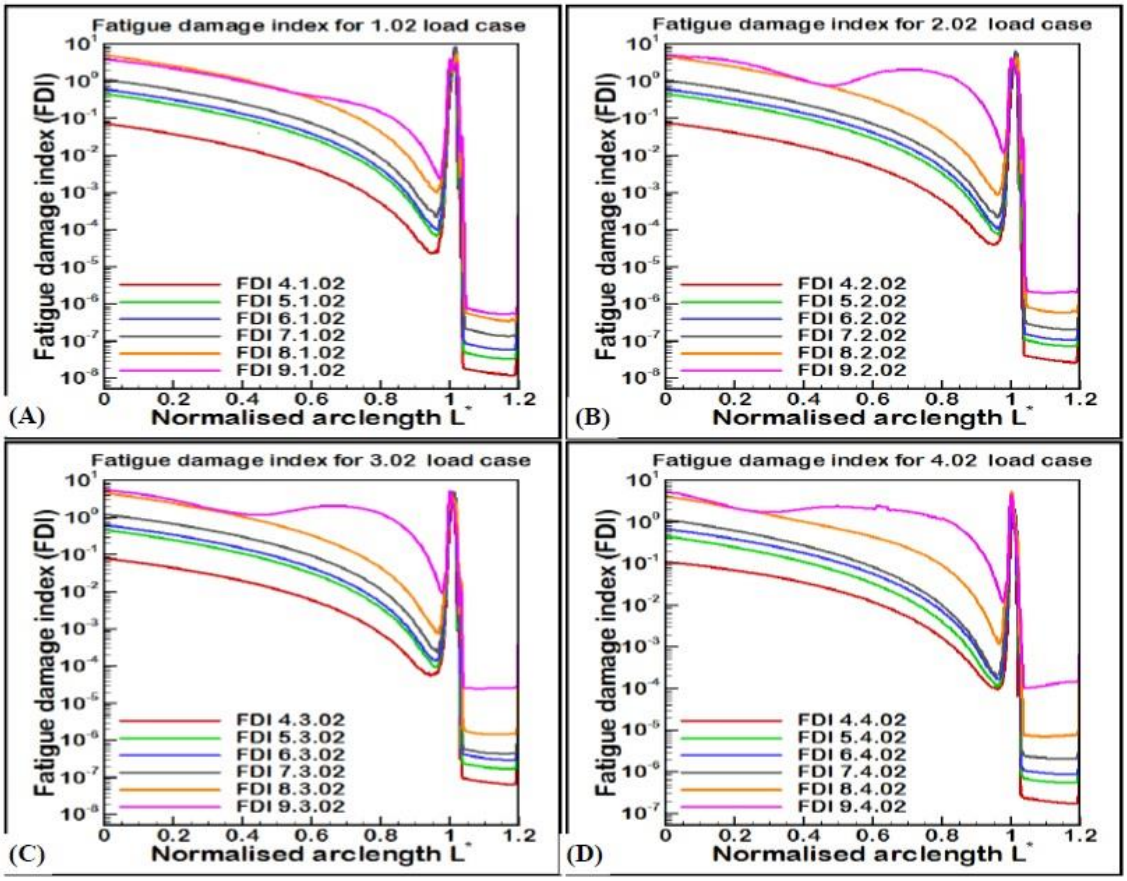

Fig. 11 Computed FDI and their comparisons under different sea states and load cases - Part 2

- The maximum computed FDI is higher under the action of power law current velocity as compared to that in linear current variation and this variation is valid for the sea state of 4, 5, 6 and 7. However, later under sea state of 8 and 9 the maximum computed FDI is higher under linear current profile as compared to that in power law current profile. The reasons of these are as explained in the previous discussion of load case 1.02 of 1.5 m/s current velocity, please refer to Fig. 11(A) and Table 7(A).

- Table 7(C) lists the magnitude and location of the maximum computer FDI for 2.0 m/s current velocity with power law variation. As before, herein we observe two peaks in each of the load cases, i.e., one is near to the connection between the offshore platform and marine riser and the second is near to the TDP. The behavior in different sea states (i.e., 4-9) is closer to the behavior observed in Table 7(B) and the explanations mentioned there holds true here too.

- Load case 4.02 under different sea states and at the current velocity of 2.25 m/s with power law: Previously, in Fig. 10(H) we have already presented the results of maximum computed FDI for 2.25 m/s current velocity under linear current variation. Now, we compute the FDI with the same loads as before but with power law variation and the results are shown in Fig. 11(D) and from them we observe the following.

Table 7 Magnitudes and locations of the computed FDI peaks for different loads (with VIV) and power law currents

Load case (with VIV)	Computed FDI (peaks)		Location (peaks)	
	Peak 1	Peak 2	Peak 1	Peak 2
(A) Power law current variation - 1.5 m/s power law current velocity with VIV.				
4.1.02	0.0755	7.3231	2.239	1011.194
5.1.02	0.076	7.768	2.985	1012.68
6.1.02	0.617	8.2760	2.240	1012.68
7.1.02	1.12	8.217	2.248	1015.67
8.1.02	4.99	5.488	5.224	1017.16
9.1.02	4.005	4.030	3.73	1000.74
(B) Power law current variation - 1.75 m/s power law current velocity with VIV.				
4.2.02	0.079	6.12	5.224	1011.94
5.2.02	0.4634	6.57	2.240	1011.94
6.2.02	0.622	6.33	2.25	1011.94
7.2.02	1.0732	6.15	2.26	1011.94
8.2.02	4.694	4.394	5.223	1015.67
9.2.02	5.109	4.255	6.716	999.25
(C) Power law current variation - 2.0 m/s power law current velocity with VIV.				
4.3.02	0.0824	4.63	2.24	1008.20
5.3.02	0.471	5.1489	2.24	1009.70
6.3.02	0.640	4.968	2.25	1009.70
7.3.02	1.217	4.75	2.20	1012.68
8.3.02	4.59	4.55	5.2238	1000.7
9.3.02	5.460	5.4088	8.20	999.25
(D) Power law current variation - 2.25 m/s power law current velocity with VIV.				
4.4.02	0.1116	1.90	5.224	1003.73
5.4.02	0.458	3.20	2.24	1002.239
6.4.02	0.6880	3.291	2.25	1002.239
7.4.02	1.144	4.936	2.26	1000.74
8.4.02	4.161	5.386	3.371	1000.74
9.4.02	5.201	4.325	3.731	997.77

- The maximum computed FDI is higher under the action of power law current velocity as compared to that in linear current variation and this variation is valid for the sea state of 4, 5, 6 and 7. However, later under sea state of 8 and 9 the maximum computed FDI is higher under linear current profile as compared to that in power law current profile. The reasons of these are as explained in the previous discussion of load case 1.02 of 1.5 m/s current velocity, please refer to Fig. 11(A) and Table 7(A).

- Table 7(D) lists the magnitude and location of the maximum computer FDI for 2.25 m/s current velocity with power law variation. As before, we observe two peaks in each of the load cases, i.e., one is near the connection between the offshore platform and marine riser and the second is near the TDP. The behavior in different sea states (i.e., 4-9) is closer to the behavior observed in Tables 7 (B) and 7(C) the explanations mentioned there hold true here too.

Table 8 Design guidelines derived from computed maximum FDI at different current velocities and load cases - Part 1

Load case (without VIV)	Computed FDI (peaks)		Location (peaks)		Length over which the computed FDI is significant other than two peaks	Lengths which are to be stiffened (m)
	Peak 1	Peak 2	Peak 1	Peak 2		
(A) Linear law current variation - 1.5 m/s current velocity in load case 1.1.						
4.1.1	0.0511	0.0013	2.238	1020.1	NA	2.238 +/- 120 m; 1020.1 +/- 120 m
5.1.1	0.2936	0.1000	2.238	1018.6	NA	2.238 +/- 120 m; 1018.6 +/- 120 m
6.1.1	0.4257	0.0295	2.238	1011.2	NA	2.238 +/- 120 m; 1011.2 +/- 120 m
7.1.1	0.8593	0.5001	2.238	1006.7	NA	2.238 +/- 120 m; 1006.7 +/- 120 m
8.1.1	3.348	3.430	8.20	1005.2	NA	8.20 +/- 120 m; 1005.2 +/- 120 m
9.1.1	2.536	2.830	2.230	1005.2	NA	2.230 +/- 120 m; 1005.2 +/- 120 m
Summary length (that is stiffened): 0 m to 129 m, 885 m to 1200 m.						
(B) Linear law current variation 1.5 m/s current velocity in load case 1.01.						
4.1.01	0.8314	0.003	2.238	1018.6	NA	2.238 +/- 120 m; 1018.6+/- 120 m
5.1.01	0.6571	0.0165	2.238	1109.7	NA	2.238 +/- 120 m; 1109.7+/- 120 m
6.1.01	0.7842	0.0290	2.238	1012.6	NA	2.238 +/- 120 m; 1012.6 +/- 120 m
7.1.01	1.2328	0.5321	2.238	1005.2	NA	2.238 +/- 120 m; 1005.2+/- 120 m
8.1.01	3.8340	2.1732	3.731	1003.3	NA	8.20 +/- 120 m; 1003.3+/- 120 m
9.1.01	5.777	1.8239	3.731	1005.2	NA	2.230 +/- 120 m; 1005.2+/- 120 m
Summary length (that is stiffened): 0 m to 124 m, 883 m to 1200 m.						
(C) Linear law current variation - 1.75 m/s current velocity in load case 2.1.						
4.2.1	0.0435	0.0010	2.23	1032.1	NA	2.23 +/- 120 m; 1032.1+/- 120 m
5.2.1	0.244	0.0080	2.23	1023.1	NA	2.23 +/- 120 m; 1023.1+/- 120 m
6.2.1	0.366	0.0231	2.23	1021.6	NA	2.23 +/- 120 m; 1021.6 +/- 120 m
7.2.1	0.833	0.3701	2.23	1017.2	NA	2.23 +/- 120 m; 1017.2 +/- 120 m
8.2.1	3.19	1.5443	2.23	1008.2	NA	2.23 +/- 120 m; 1008.2+/- 120 m
9.2.1	2.541	2.91	7.46	1014.1	NA	7.46 +/- 120 m; 1014.1 +/- 120 m
Summary length (that is stiffened): 0 m to 128 m, 888 m to 1200 m.						
(D) Linear law current variation.						
4.2.01	6.855	---	2.23	---	NA	2.23 +/- 120 m; ----
5.2.01	0.973	0.0098	2.23	1024.62	NA	2.23 +/- 120 m; 1024.62 +/- 120 m
6.2.01	1.8153	0.025	2.23	1024.62	NA	2.23 +/- 120 m; 1024.62 +/- 120 m
7.2.01	7.4598	0.382	2.23	1021.64	NA	2.23 +/- 120 m; 1021.64 +/- 120 m
8.2.01	8.634	0.729	3.73	1026.11	NA	3.73 +/- 120 m; 1026.11+/- 120 m
9.2.01	8.34	1.3092	2.23	1023.13	NA	2.23 +/- 120 m; 1023.13 +/- 120 m
Summary length (that is stiffened): 0 m to 124 m, 900 m to 1200 m. NA: Not applicable. Upper restricted length = 0 m, and Lower restricted length = 1200 m.						

7.3 Visual presentation of the simulation at TDP

Figs. 12 (A)-12(I) show the movement of the TDP of the marine riser during the simulation from 21 s to 29 s. Here we have reported only a certain segment of the time domain simulation i.e., from 21 sec to 29 s. However it is possible to show similar graphics for the larger time of the simulation.

From Figs. 12 (A)-12(I) it can be noted that as the simulation proceeds the TDP comes under the

action of the loads 8.4.01 as listed in Table 5(D). As we can see that the TDP is continuously under the action of the repeated cycles of tension and compression, it is one of the major locations where the FDI is higher. The segment of the riser is on the sea bed is marked in white color and the segment of the riser in yellow color is lifted part of the riser.

8. Conclusions

8.1 Static analysis

We can conclude the following:

- Each of the even modes is dominating only in the in-line and axial directions rather than in the transverse direction, and each of the odd modes is dominating in the transverse direction compared to the axial and in-line directions. In the even number modes, the contribution of inline motion is significant along with a fair contribution from the axial motion, and this distribution remains more or less the same even at the higher even number of modes.
- All the odd number modes are dominated by the transverse motions and other contributions are non-significant (i.e. close to 0) and this implies that the odd number of modes will be easier to address for fatigue damage control in comparison to the even number of modes.

8.2 Dynamic analysis

Our presented results show and analyze the influences of VIV and different current variations and they offer deep and meaningful insights into the computed FDI for a combination of loads, i.e., wave, current and VIV.

8.3 FDI for the cases of without and with VIV

8.3.1 Linear law variation

We can conclude the following:

- In all the results, we observe multiple peaks of the computed FDI, i.e., one peak is close to the top end connection of the offshore platform and marine riser and the second peak is close to the TDP.
- The dominance of a particular peak depends upon the sea state, current velocity, and VIV and it shows a wide variation.
- The VIV generates motions that are periodic/oscillatory and depending upon the matching of amplitudes and phase differences between different motion waves, there can be a coupling of motions because of the waves and VIV. Once this happens, this will result into the computed higher FDI, e.g., load cases 2.01 and 2.1, etc.

8.3.2 Power law variation

We can conclude the following:

- In general, especially in the low to medium sea states (i.e., 4, 5, 6, and 7) the maximum computed FDI is higher under the action of power law current velocity than that in linear current variation. However, later under sea states of 8 and 9 the maximum computed FDI is either higher under linear current profile or closer to it than that in power law current profile.

Table 9 Design guidelines derived from computed maximum FDI at different current velocities and load cases - Part 2

Load case (without VIV)	Computed FDI (peaks)		Location (peaks)		Length over which the computed FDI is significant other than two peaks	Lengths which are to be stiffened (m)
	Peak 1	Peak 2	Peak 1	Peak 2		
(A) Linear law current variation.						
4.3.1	0.0396	0.0007	2.238	1047.0	NA	2.238 +/- 120 m; 1047.0+/- 120 m
5.3.1	0.199	0.0046	2.238	1039.5	NA	2.238 +/- 120 m; 1039.5+/- 120 m
6.3.1	0.329	0.0156	2.238	1038.0	NA	2.238 +/- 120 m; 1038.0 +/- 120 m
7.3.1	0.861	0.3181	2.238	1032.0	NA	2.238 +/- 120 m; 1032.0 +/- 120 m
8.3.1	5.617	2.340	2.238	1024.6	NA	2.238 +/- 120 m; 1024.6+/- 120 m
9.3.1	3.231	2.218	2.238	1035.0	NA	2.238 +/- 120 m; 1035.0 +/- 120 m
Summary length (that is stiffened): 0 m to 123 m, 904 m to 1200 m.						
(B) Linear law current variation.						
4.3.01	0.229	0.0013	2.238	1051.5	NA	2.238 +/- 120 m; 1051.5+/- 120 m
5.3.01	0.452	0.0057	2.238	1051.5	NA	2.238 +/- 120 m; 1051.5+/- 120 m
6.3.01	0.930	0.0197	2.238	1042.6	NA	2.238 +/- 120 m; 1042.6 +/- 120 m
7.3.01	2.013	0.3058	2.238	1035.1	NA	2.238 +/- 120 m; 1035.1 +/- 120 m
8.3.01	5.40	0.8211	2.238	1041.4	NA	2.238 +/- 120 m; 1041.4+/- 120 m
9.3.01	9.67	1.394	2.238	1042.5	NA	2.238 +/- 120 m; 1042.5+/- 120 m
Summary length (that is stiffened): 0 m to 123 m, 915 m to 1200 m.						
(C) Linear law current variation.						
4.4.1	0.039	0.0007	2.238	1069.4	NA	2.238 +/- 120 m; 1069.4+/- 120 m
5.4.1	0.190	0.0039	2.238	1067.9	NA	2.238 +/- 120 m; 1067.9+/- 120 m
6.4.1	0.321	0.0124	2.238	1063.4	NA	2.238 +/- 120 m; 1063.4 +/- 120 m
7.4.1	0.888	0.3150	2.238	1045.5	NA	2.238 +/- 120 m; 1045.5+/- 120 m
8.4.1	3.685	1.930	2.238	1045.5	NA	2.238 +/- 120 m; 1045.5+/- 120 m
9.4.1	5.111	3.736	2.238	1041.0	NA	2.238 +/- 120 m; 1041.0+/- 120 m
Summary length (that is stiffened): 0 m to 123 m, 920 m to 1200 m.						
(D) Linear law current variation.						
4.4.01	0.1104	0.002	2.238	1073.8	NA	2.238 +/- 120 m; 1073.8+/- 120 m
5.4.01	0.5267	0.009	2.238	1072.3	NA	2.238 +/- 120 m; 1072.3+/- 120 m
6.4.01	0.613	0.0241	2.238	1067.9	NA	2.238 +/- 120 m; 1067.9 +/- 120 m
7.4.01	1.453	0.3056	2.238	1057.4	NA	2.238 +/- 120 m; 1057.4+/- 120 m
8.4.01	11.039	1.216	2.238	1061.9	NA	2.238 +/- 120 m; 1061.9 +/- 120 m
9.4.01	16.732	2.60	2.238	1054.5	NA	2.238 +/- 120 m; 1054.5+/- 120 m
Summary length (that is stiffened): 0 m to 124 m, 900 m to 1200 m. NA: Not applicable. Upper restricted length = 0 m, and Lower restricted length = 1200 m.						

- Computed results of FDI show that the FDI behavior under the combined effects of wave, current and VIV is highly complex, non-linear and defies simple explanations regarding monotonic increase or decrease.

This higher added mass is because of the predominance of lower current velocities across a larger length of marine riser in the case of power law as compared to the linear law. We have already shown that in linear law, the decrease in current velocity is very low compared to the power law.

Table 10 Design guidelines derived from computed maximum FDI at different current velocities and load cases - Part 3

Load case (without VIV)	Computed FDI (peaks)		Location (peaks)		Length over which the computed FDI is significant other than two peaks	Lengths which are to be stiffened (m)
	Peak 1	Peak 2	Peak 1	Peak 2		
(A) Power law current variation.						
4.1.2	0.073	6.781	2.24	1012.0	NA	2.240 +/- 120 m; 1012.0+/- 120 m
5.1.2	0.455	6.403	2.25	1012.0	NA	2.25 +/- 120 m; 1012.0 +/- 120 m
6.1.2	0.574	7.236	2.22	1014.79	NA	2.22 +/- 120 m; 1014.79 +/- 120 m
7.1.2	1.055	8.405	2.24	1015.56	NA	2.24 +/- 120 m; 1015.56 +/- 120 m
8.1.2	5.922	5.290	5.22	1015.56	NA	5.22 +/- 120 m; 1015.56 +/- 120 m
9.1.2	4.280	4.090	5.25	999.25	NA	5.22 +/- 120 m; 999.25 +/- 120 m
Summary length (that is stiffened): 0 m to 126 m, 880 m to 1200 m.						
(B) Power law current variation.						
4.1.02	0.0755	7.3231	2.239	1011.19	NA	2.239 +/- 120 m; 1011.19+/- 120 m
5.1.02	0.076	7.768	2.985	1012.68	NA	2.985 +/- 120 m; 1012.68 +/- 120 m
6.1.02	0.617	8.2760	2.240	1012.68	NA	2.240 +/- 120 m; 1012.68 +/- 120 m
7.1.02	1.12	8.217	2.248	1015.67	NA	2.248 +/- 120 m; 1015.67 +/- 120 m
8.1.02	4.99	5.488	5.224	1017.16	NA	5.224 +/- 120 m; 1017.16 +/- 120 m
9.1.02	4.005	4.030	3.730	1000.74	570-970	3.730 +/- 120 m; 1000.74 +/- 120 m
Summary length (that is stiffened): 0 m to 126 m, 880 m to 1200 m.						
(C) Power current variation.						
4.2.2	0.069	5.193	2.240	1011.2	NA	2.240 +/- 120 m; 1011.2 +/- 120 m
5.2.2	0.391	5.270	2.240	1012.6	NA	2.240 +/- 120 m; 1012.6 +/- 120 m
6.2.2	0.551	6.257	2.240	1012.6	NA	2.240 +/- 120 m; 1012.6 +/- 120 m
7.2.2	0.993	7.182	2.240	1014.8	NA	2.240 +/- 120 m; 1014.8 +/- 120 m
8.2.2	5.349	4.228	5.220	1015.6	NA	5.220 +/- 120 m; 1015.6 +/- 120 m
9.2.2	3.757	4.435	3.731	999.28	NA	3.731 +/- 120 m; 999.28 +/- 120 m
Summary length (that is stiffened): 0 m to 126 m, 870 m to 1200 m.						
(D) Power law current variation.						
4.2.02	0.079	6.12	5.224	1011.94	NA	5.224 +/- 120 m; 1011.94+/- 120 m
5.2.02	0.4634	6.57	2.240	1011.94	NA	2.240 +/- 120 m; 1011.94 +/- 120 m
6.2.02	0.622	6.33	2.25	1011.94	NA	2.250 +/- 120 m; 1011.94 +/- 120 m
7.2.02	1.0732	6.15	2.26	1011.94	NA	2.260 +/- 120 m; 1011.94 +/- 120 m
8.2.02	4.694	4.394	5.223	1015.67	NA	5.223 +/- 120 m; 1015.67 +/- 120 m
9.2.02	5.109	4.255	6.716	999.25	460-970	6.716+/- 120 m; 999.25 +/- 120 m
Summary length (that is stiffened): 0 m to 127 m, 870 m to 1200 m. NA: Not applicable. Upper restricted length = 0 m, and Lower restricted length = 1200 m.						

Apart from the observations as mentioned above, we note the following design recommendations:

- The design for FDI is specific to the sea state, current velocity, VIV and the law of variation. A proper design looks at the specific combinations of loads and design and strengthen accordingly.

- The lengths around the computed maximum FDI (i.e., peaks) need to be stiffened and a rule of thumb is +/- 10%. These lengths that are needed to be stiffened are listed in Tables 8-11. We

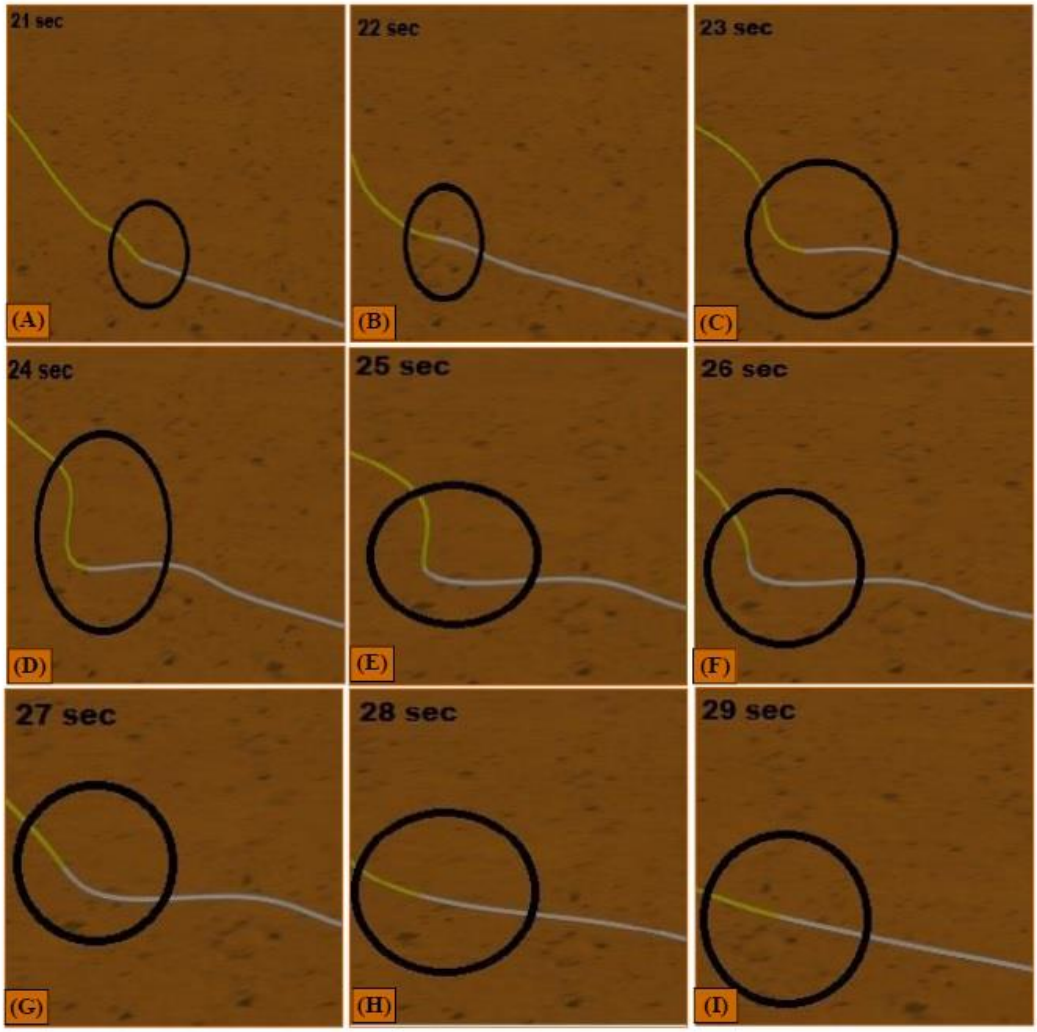

Fig. 12 Visual representation of the simulation for 8.4.01 load case

note that in actual practice the final application in design is the combined lengths that are derived from Table 8 to 11 and it implies that the marine riser will be stiffened from 0 m 129 m and from 870 m to 1200 m accounting for the sea states 4 to 9, current velocities from 1.5 m/s to 2.25 m/s and with/without the VIV.

- A power law variation is more representative of the real world current variation and because of this it is more meaningful to design for the FDI based upon the results of power law variation, i.e. load cases 1.02, 2.02, 3.02 and 4.02.

- Although, this will result into an economical and efficient design, because the marine engineering community is highly conservative a design with results from linear law will be more acceptable to the order placing agencies/clients.

- A linear law results into over prediction of the computed FDI and because of this the designs from this law will always result into bulkier marine structures.

Table 11 Design guidelines derived from computed maximum FDI at different current velocities and load cases - Part 4

Load cases	Computed FDI (peaks)		Location (peaks)		Length over which the computed FDI is significant other than two peaks	Lengths which are to be stiffened (m)
	Peak 1	Peak 2	Peak 1	Peak 2		
(A) Power law current variation. ***Load case - without VIV.***						
4.3.2	0.065	4.210	2.240	1009.7	NA	2.240 +/- 120 m; 1009.7+/- 120 m
5.3.2	0.371	4.461	2.240	1009.7	NA	2.240 +/- 120 m; 1009.7 +/- 120 m
6.3.2	0.530	5.352	2.240	1009.7	NA	2.240 +/- 120 m; 1009.7 +/- 120 m
7.3.2	0.965	4.865	2.240	1012.6	NA	2.240 +/- 120 m; 1012.6 +/- 120 m
8.3.2	4.785	4.506	5.220	1002.4	NA	5.220 +/- 120 m; 1002.4 +/- 120 m
9.3.2	3.483	5.226	3.737	999.25	NA	3.737 +/- 120 m; 999.25 +/- 120 m
Summary length (that is stiffened): 0 m to 126 m, 870 m to 1200 m.						
(B) Power law current variation. ***Load case – with VIV.***						
4.3.02	0.0824	4.63	2.24	1008.20	NA	2.240 +/- 120 m; 1008.94+/- 120 m
5.3.02	0.471	5.1489	2.24	1009.70	NA	2.240 +/- 120 m; 1009.70 +/- 120 m
6.3.02	0.640	4.968	2.25	1009.70	NA	2.250 +/- 120 m; 1009.70 +/- 120 m
7.3.02	1.217	4.75	2.20	1012.68	NA	2.20 +/- 120 m; 1012.94 +/- 120 m
8.3.02	4.59	4.55	5.2238	1000.7	NA	5.2238 +/- 120 m; 1007.7 +/- 120 m
9.3.02	5.460	5.4088	8.20	999.25	400-970	8.20+/- 120 m; 999.25 +/- 120 m
Summary length (that is stiffened): 0 m to 129 m, 880 m to 1200 m.						
(C) Power current variation. ***Load case - without VIV.***						
4.4.2	0.620	0.913	2.300	1003.70	NA	2.300+/- 120 m; 1003.70+/- 120 m
5.4.2	0.346	1.992	2.280	1000.70	NA	2.280 +/- 120 m; 1000.70 +/- 120 m
6.4.2	0.501	2.949	2.280	1002.23	NA	2.280 +/- 120 m; 1002.23+/- 120 m
7.4.2	0.930	4.433	2.280	999.25	NA	2.280+/- 120 m; 999.25 +/- 120 m
8.4.2	4.145	5.929	5.220	999.25	NA	5.220 +/- 120 m; 999.25 +/- 120 m
9.4.2	3.420	4.025	3.731	999.25	280-970	3.731 +/- 120 m; 999.25 +/- 120 m
Summary length (that is stiffened): 0 m to 126 m, 879 m to 1200 m.						
(D) Power law current variation. ***Load case – with VIV.***						
4.4.02	0.1116	1.90	5.224	1003.73	NA	5.224 +/- 120 m; 1003.73+/- 120 m
5.4.02	0.458	3.20	2.24	1002.23	NA	2.240 +/- 120 m; 1002.23 +/- 120 m
6.4.02	0.6880	3.291	2.25	1002.23	NA	2.250 +/- 120 m; 1002.23 +/- 120 m
7.4.02	1.144	4.936	2.26	1000.74	NA	2.26 +/- 120 m; 1000.74 +/- 120 m
8.4.02	4.161	5.386	3.371	1000.74	NA	3.371 +/- 120 m; 1007.74 +/- 120 m
9.4.02	5.201	4.325	3.731	997.77	280-970	3.371+/- 120 m; 997.77 +/- 120 m
Summary length (that is stiffened): 0 m to 126 m, 877 m to 1200 m. NA: Not applicable. Upper restricted length = 0 m, and Lower restricted length = 1200 m.						

8.4 Future scope of research

Although, all the loads considered in this work are highly random and probabilistic in the nature, neither their randomness nor their probabilistic natures have been investigated in the present analysis. We note that only for the wave data in sea states a random nature has been considered, i.e., JONSWAP spectrum.

It is agreed that the real oceans do not have any specific sea state occurrence at any particular time and the real distribution is a combination of different sea states, and there will be a probabilistic distribution with respect to time. Although, this probabilistic approach is expected to represent the real world ocean data, this has not been attempted in the present thesis as the present work is the first step towards building a computer based simulation model for the fatigue damage assessment of deep water marine riser here at the DOE, IIT Madras, India. In future, this approach will be adopted.

Presented CSM can be extended to incorporate the random and probabilistic modules and then a detailed sensitivity analysis can be done specific to a location, design life and conditions. Furthermore, the presented CSM will need proper and detailed verification and validation from more results from either experiments or computations or both along with field data and filters. Herein, we have shown that in general the 'Fatigue Damage Index (FDI)' of the marine riser depends on multiple parameters, i.e., current velocity, current profile, 'Vortex Induced Vibration (VIV)', and platform motions, etc. Although, in general it is believed that the 'Touch Down Point (TDP)' will have the highest FDI, we note and have shown herein that the FDI is cumulative and each of the parameters contribute to it through the principles of superimposition and coupling. In some specific load cases the maximum FDI shifts from the TDP to different fairlead positions because of the stochastic nature of current velocity, current profile, the VIV and platform motions, etc. As these are coupled and superimposed effects, they get added up in some cases and get cancelled also in some cases. As a limitation, we note here that in what cases they get added up and in what cases they get cancelled, have not been investigated in the present paper.

This is being planned to be considered as a separate research problem from design point of view. From the present study, we can conclude that from the design point of view it is not only the TDP which will suffer from the higher FDI but depending upon the loading conditions the fairlead point can also have the higher FDI. In the integrated dynamic analysis of marine riser and offshore platform system, a mode weighted analysis might be more practical in design.

Also, the effect of the short crestedness can be considered for the design and development of a more detailed design approach. Even though all the oceanic loads are considered in the present work, other loads like functional loads, and accidental loads, etc., are not considered by us.

Our future works shall go in these directions and some of them are currently under investigation by us.

Trademark and copyrights

Acknowledgements

This research was supported by the internal research grants of IIT Madras, India via a scheme - OE14S006 and a scholarship scheme of the MHRD, GoI, India.

References

Ahmad, S. and Datta, T.K. (1989), "Dynamic response of marine risers", *Eng. Struct*., **11**(3), 179-188. https://doi.org/10.1016/0141-0296(89)90005-9.

Beer, F.P., Russell, E., Johnston, J.R., Dewolf, J.T. and Mazurek D.F. (2016), *Mechanics of Materials,* 6th edition, McGraw-Hill Science Engineering, USA.

Blevins R. D. (2001), Flow-Induced Vibration, Krieger Publishing Company, USA.

Bokaian, A. (1990), "Natural frequencies of beams under tensile axial loads", *J. Sound Vib.*, **142**(3), 481-498. https://doi.org/10.1016/0022-460X(90)90663-K.

Campbell, M. (1999), "The complexities of fatigue analysis for deepwater risers", *Proceedings of the Deepwater Pipeline Conference*, New Orleans, USA.

Cengel, Y.A. and Cimbala, J.M. (2017), *Fluid Mechanics: Fundamentals and Applications,* 4th Ed., McGraw-Hill Education, USA.

Chen, W., Li, M., Guo, S. and Gan, K. (2014), "Dynamic analysis of coupling between floating top-end heave and riser's vortex-induced vibration by using finite element simulations", *Appl. Ocean Res.,* **48,** 1-9. https://doi.org/10.1016/j.apor.2014.07.005.

Coe, R.G. and Neary, V.S. (2014), "Review of methods for modelling wave energy converter survival in extreme sea states", *Proceedings of the 2nd Marine Energy Technology Symposium (METS 2014)*, Seattle, WA, USA, April 15-18.

Dahlquist, G. and Björck, Å (2003), *Numerical Methods,* Dover Publications, UK.

Danielssen, D.S., Edler, L, Fonselius, S., Henroth, L, Ostrowski, M, Svendsen, E. and Talpsepp, L. (1997). "Oceanographic variability in the skagerrak and northern kattegat, may-june, 1990 - international council for the exploration of the sea", *J. Mar. Sci.*, **54**(5), 753-773. https://doi.org/10.1006/jmsc.1996.0210.

Domala, V., Ranjeet, M. and Sharma, R. (2014), "A Note on Effect of Geometric Dimensions, Shape and Arrangement of Columns and Pontoons on Heave and Pitch Response of Semi-Submersible", *Proceedings of the MTS/IEEE Oceans*.

Faltinsen, O.M. (1993), *Sea Loads on Ships and Offshore Structures*, Cambridge Ocean Technology Series, Cambridge University Press, UK.

Fleck, N.A., Shin, C.S. and Smith, R.A. (1985), "Fatigue crack growth under compressive loading", *Eng. Fract. Mech.*, **21**(1), 173-185. https://doi.org/10.1016/0013-7944(85)90063-3.

Gao, Y., Zong, Z. and Sun, L. (2011), "Numerical prediction of fatigue damage in steel catenary riser due to vortex-induced vibration", *J. Hydrodynam.*, **23**(2), 154-163. https://doi.org/10.1016/S1001-6058(10)60099-6.

Gosain, G.D., Sharma, R. and Kim, T.W. (2017), "An optimization model for preliminary stability and configuration analyses of semi-submersibles", *Int. J. Maritime Eng. (IJME)*, **159**(3), 249-270. https://doi.org/10.5750/ijme.v159iA3.

Gordon, A. (1967), "Circulation of the Caribbean sea", *J. Geophys. Res*., **72**(24), 6207-6223. https://doi.org/10.1029/JZ072i024p06207.

Hasselmann, K. (1966), "Feynman diagrams and interaction rules of wave-wave scattering processes", *Review. Geophys*., **4**(1), 1-32. https://doi.org/10.1029/RG004i001p00001.

Hasselmann, K., Barnett, T.P., Bouws, E., Carlson, H., Cartwright, D.E., Enke, K., Ewing, J.A., Gienapp, H., Hasselmann, D.E., Kruseman, P., Meerburg, A., Muller, P., Olbers, D.J., Richter, K., Sell, W. and Walden, H. (1973), "Measurement of wind–wave growth and swell decay during the joint north sea wave project (jonswap), UDC 551.466.31, ANE German Bight", *Erganzunscheftzur Deutschen Hydrographischen Zeitschrift, Reihe*, *A***, 80**, 1-95.

Howells, H. (1995), "Advances in steel catenary riser design", *Proceeding of the 2nd Annual International Forum on Deepwater Technology,* Aberdeen, February.

Huarte, F.H., Bearman, P.W. and Chaplin, J.R. (2006), "On the force distribution along the axis of a flexible circular cylinder undergoing multi-mode vortex-induced vibrations", *J. Fluid. Struct.*, **22**(6-7), 897-903. https://doi.org/10.1016/j.jfluidstructs.2006.04.014.

Iwan W.D. and Blevins, R.D. (1974), "A model for vortex induced oscillation of structures", *J. Appl. Mech.*, **41**(3), 581-586. https://doi.org/10.1115/1.3423352.

Jauvits, N. and Williamson, C.H.K. (2004), "The effect of two degrees of freedom on vortex-induced vibration at low mass and damping", *J. Fluid Mech.*, **50**, 23-62. https://doi.org/10.1017/S0022112004008778.

Journée, J.M. and Massie, W.W. (2001), Offshore hydromechanics, 1st Ed., *Delft University of Technology,* The Netherlands.

Khan, R.A., Kaur, A., Singh, S.P. and Ahmad, S. (2011), "Nonlinear dynamic analysis of marine risers under random loads for deep-water fields in Indian offshore", *Procedia Eng.*, **14**, 1334-1342, https://doi.org/10.1016/j.proeng.2011.07.168.

Kim, W.H. and Laird, C. (1978), "Crack nucleation and stage I propagation in high strain fatigue - II. Mechanism", *Acta Metallurgica*, **26**(5), 789-799. https://doi.org/10.1016/0001-6160(78)90029-9.

Lei, S., Zhang, W.S., Lin, J.H., Yue, Q.J., Kennedy, D. and Williams, E.F. (2014), "Frequency domain response of a parametrically excited riser under random wave forces", *J. Sound Vib.*, **333**(2), 485-498. https://doi.org/10.1016/j.jsv.2013.09.025.

Lieurade, H.P. (1989), *Fatigue Analysis in Offshore Structures,* (Eds., Branco, C.M., Rosa, L.G.), Advances in Fatigue Science and Technology, NATO ASI Series (Series E: Applied Sciences), 159, Springer, Dordrecht.

Ljuština, A.M., Parunov, J. and Senjanović, I. (2004), "Static and dynamic analysis of marine riser", *Proceedings of the 16th Symposium of Theory and Practice of Shipbuilding*, Sorta.

Mekha, B.B. (2001), "New frontiers in the design of steel catenary risers for floating production systems", *J. Offshore Mech.Arct. Eng.*, **23**(4), 153-158. https://doi.org/10.1115/1.1410101.

Miliou, A., Vecchi, A.D.E., Sherwin, S.J. and Graham, J.M.R. (2007), "Wake dynamics of external flow past a curved circular cylinder with the free stream aligned with the plane of curvature", *J. Fluid Mech.*, **592**, 89-115. https://doi.org/10.1017/S0022112007008245.

Modarres-Sadeghi, Y., Mukundan, H., Dahl, J.M., Hover, F.S. and Triantafyllou, M.S. (2010), "The effect of higher harmonic forces on fatigue life of marine risers", *J. Sound Vib.*, **329(1)**, 43-55. https://doi.org/10.1016/j.jsv.2009.07.024.

Morooka, C.K. and Tsukada, R.I. (2013), "Experiments with a steel catenary riser model in a towing tank", *Appl. Ocean Res.*, **43**, 244-255. https://doi.org/10.1016/j.apor.2013.10.010.

Naudascher, E. and Rockwell, D. (2005), *Flow-Induced Vibrations: An Engineering Guide*, Dover Civil and Mechanical Engineering Series, Dover Publications, UK.

Newman, J.N. (2018), *Marine Hydrodynamics*, Anniversary edition, The MIT Press, USA.

Pallan, C.A. (2019), "A Computer Based Simulation Model for the Fatigue Damage Assessment of Deep Water Marine Riser", Master of Science (By Research) Thesis, Department of Ocean Engineering, IIT Madras, India.

Rivero-Angeles, F.J., Vázquez-Hernández, A.O. and Sagrilo, L.V.S. (2013), "Spectral analysis of simulated acceleration records of deep-water SCR for identification of modal parameters", *Ocean Eng.*, **58**, 8-87. https://doi.org/10.1016/j.oceaneng.2012.10.010.

Roveri, F.E. and Vandiver, J.K. (2001), "Slenderex: Using Shear7 for Assessment of Fatigue Damage Caused by Current Induced Vibrations", *Proceedings of the 20th International Conference on Offshore Mechanics and Arctic Engineering*, Rio de Janeiro, Brazil, June 3-8.

Schijve, J. (2009), *Fatigue of structures and materials*, 2nd edition, Springer Netherlands.

Srinil, N. (2011), "Analysis and prediction of vortex-induced vibrations of variable-tension vertical risers in linearly sheared currents", *Appl. Ocean Res.*, **33**(1), 41-53. https://doi.org/10.1016/j.apor.2010.11.004.

Sturges, W. and Leben, R. (2000), "Frequency of ring separations from the loop current in the Gulf of Mexico: a revised estimate", *J. Phys. Oceanography*, **30**(7), 1814-1819. https://doi.org/10.1175/1520-0485(2000)030<1814:FORSFT>2.0.CO;2.

Talka (1981), "The Alexander L. Kielland Accident", March 1981:11, Report Of A Norwegian Public Commission Appointed By Royal Decree Of March 28, 1980, Ministry of Justice and Police, Norwegian Public Reports.

Techet, A.H. (2005), Design Principles for Ocean Vehicles, Lecture notes - 13.42, Department of Mechanical

Engineering, MIT, USA.
Thomson, W. (2004), "*Theory of Vibration with Applications*", 1st Ed., CRC Press, USA.
TMAA (2014), Technical Manual (Version 14.0). ANSYS Incorporated, Canonsburg, PA, USA.
TMO (2013), Technical Manual Orcaflex (Version 7), Orcina Limited, London, USA.
Ulveseter, J.V., Thorsen, M.J., Sævik, S. and Larsen, C.M. (2018), "Time domain simulation of riser VIV in current and irregular waves", *Mar. Struct.*, **60**, 241-260. https://doi.org/10.1016/j.marstruc.2018.04.001.
Vandiver, J.K. (1983), "Drag coefficients of long flexible cylinders", *Proceedings of the Offshore Technology Conference*, Houston, Texas, May.
Vikestad, K., Larsen, C.M. and Vandiver, J.K. (2000), "Norwegian deepwater program: damping of vortex-induced vibrations", *Proceeding of the Offshore Technology Conference*, Houston, Texas, May.
Vandiver, J.K. and Chung, T.Y. (1988), "Predicted and measured response of flexible cylinders in sheared flow", *Proceedings of the ASME Annual Meeting Symposium on Flow-Induced Vibration*, Chicago, November.
Vandiver, J.K., Swithenbank, S.B., Jaiswal, V. and Jhingran, V. (2006), "Fatigue damage from high mode number vortex-induced vibration", *Proceedings of the 25th International Conference on Offshore Mechanics and Arctic Engineering*, Hamburg Germany, June 4-9.
Varvani-Farahani, A. (2005), *Advances in Fatigue, Fracture and Damage Assessment of Materials, Series on Advances in Damage Mechanics*, WIT Press, USA.
Wang, K., Xue, H., Tang, W. and Guo, J. (2013), "Fatigue analysis of steel catenary riser at the touch-down point based on linear hysteretic riser-soil interaction model", *Ocean Eng.*, **68**, 102-111. https://doi.org/10.1016/j.oceaneng.2013.04.005.
Watters, A.J., Smith, L.C. and Garrett, D.L. (1998), "The lifetime dynamics of a deep water riser design", *Appl. Ocean Res.*, **20**(1-2), 69-81. https://doi.org/10.1016/S0141-1187(98)00011-X.
White F. M. (2015), *Fluid Mechanics,* 8th edition, McGraw-Hill Education, USA.
Wu, X., Ge, F. and Hong, Y. (2012), "A review of recent studies on vortex-induced vibrations of long slender cylinders", *J. Fluid. Struct.*, **28**, 292-308. https://doi.org/10.1016/j.jfluidstructs.2011.11.010.
Xue, H., Tang, W. and Qu, X. (2014), "Prediction and analysis of fatigue damage due to cross-flow and in-line viv for marine risers in non-uniform current", *Ocean Eng.*, **83**, 52-62. https://doi.org/10.1016/j.oceaneng.2014.03.023.
Zhang, B. and Qiu, W. (2018), "Improving time-domain prediction of vortex-induced vibration of marine risers", *Mar. Syst. Ocean Technol.*, **13**(1), 13-25. https://doi.org/10.1007/s40868-017-0041-3.

MK

Nomenclature

A =Amplitude of motion of the marine riser,
A_w = Water plane area,
A_i and A_0 = Internal and external areas of the deep water marine riser
b = Slope of S-N curve,
B_{CG} = Buoyancy at the 'Centre of Gravity (CoG)',
c = System linear damping of semisubmersible,
C = Curvature of marine riser,
C_t = Torsional damping coefficient of marine riser,
$C_r(p_r, v_r)$ = Marine riser damping load,
d = Water depth,
D_c = Critical damping for bending,
D_i = Fatigue Damage Index (FDI),
dL/dt = Rate of change of length with respect to time,
$\left(d\tau/dt\right)$ = Rate of change of twist w.r.t. time,
e = Damping coefficient in the tension,
EA = Axial stiffness of riser,
EI = Bending stiffness of marine riser,
ds = Small element of semi-submersible surface,
F (t) = External excitation force,
F_{Hys} = Hydrostatic force,
F_j = Force in j^{th} direction and n_j is the normal vector to j^{th} element,
F_{ji} = Force in i^{th} direction due to motion in j^{th} degree of freedom,
g = Acceleration due to gravity,
k_s = Total stiffness of the semisubmersible,
k_t = Torsional stiffness of marine riser,
k_r = Marine riser element stiffness,
$k_r(p_r)$ = Mariner riser stiffness load,
L = Length of segment of marine riser,
L_0 = Un-stretched length,
L^* = Normalized riser length with Touch Down point (TDP),
M (r) = Mass of marine riser (including the added mass),
$M_r(p_r, a_r)$ = Marine riser's inertia load (including added mass),
M (a) = Hydrodynamic added mass of semisubmersible,
M (s) = Mass of semisubmersible,
N_i = Number of stress cycles applied,
N_{fi} = Minimum number of stress cycles needed to cause failure under that class of load,
N_1 and N_2 = Load cycles corresponding to the S_1 and S_2 stress level,
M_{Hys} = Hydrostatic moment,
$\vec{n}$ = Surface unit normal of semi-submersible,
p = Pressure distribution,
p_i and p_0 = Internal and external pressures in the deep water marine riser,

(p,q,r) = finite angular rotation of semi-submersible,

p_r, v_r and a_r = Position, velocity and acceleration at any specify time t on the marine riser element,

r = Distance from center of semi-submersible,

ρ = Sea water density,

$S^{+}(w)$ = Frequency dependent spectral energy,

T_e = Effective tension in riser,

u_s = Wind speed at 10m above sea surface,

V_n = Velocity normal to surface,

w = Angular frequency of the wave spectrum,

w_m = Peak spectral frequency,

X = RAO of semisubmersible,

$X^{(1)}$ = New position of semi-submersible,

x_s = Fetch distance,

α = A constant depending upon the wind velocity,

ε = Axial strain,

Φ = Total flow potential,

Φ_s = Total scattered wave potential,

Φ_i = Total incident wave potential,

Φ_j = Total radiated wave potential,

ϕ = Spatial flow potential,

ϕ_s = Spatial scattered wave potential,

ϕ_i = Spatial incident wave potential,

ϕ_j = Spatial radiated potential due to motion in the j^{th} degree of freedom (x_j),

γ = Shape factor of spectrum,

λ = Eigen value,

λ_t = Target bending damping,

η = Instantaneous wave surface elevation,

τ = Segmental twist angle,

υ = Poisson ratio,

ω = Natural circular frequency of the semi-submersible, and

ω_{nr} = Natural circular frequency of marine riser.